JOURNAL OF GUIDANCE, CONTROL, AND DYNAMICS
Vol. 43, No. 12, December 2020

Structured μ-Synthesis of Robust Attitude Control Laws for Quad-Tilt-Wing Unmanned Aerial Vehicle

Simone Panza* and Marco Lovera†
Politecnico di Milano, Milan 20156, Italy
and
Masayuki Sato‡ and Koji Muraoka‡
Japan Aerospace Exploration Agency, Tokyo 181-0015, Japan

https://doi.org/10.2514/1.G005080

The problem of designing the longitudinal flight controller for a quad-tilt-wing unmanned aerial vehicle to achieve robust performance under constraints on the controller structure is considered. An approach based on μ-synthesis is proposed, in which a nonparametric inverse multiplicative uncertainty description is employed to account for the uncertainties of the aircraft attitude dynamics at each operating condition, with specific reference to variations in the number of unstable modes. The resulting μ-synthesis problem with a frequency-dependent weighting function, the structure of which is defined a priori, is reformulated as a structured H_∞ problem and solved by means of available MATLAB software. Simulation results are presented in order to show the effectiveness of the approach.

Nomenclature

K	=	number of design points
q	=	pitch rate, rad/s
T	=	set of nominal and perturbed operating conditions
T_p	=	set of perturbed operating conditions
$W_S(s)$	=	performance weighting function, i.e., weighting function for sensitivity function
$W_U(s)$	=	uncertainty weighting function
θ	=	pitch angle, rad
τ_w	=	wing tilt angle, deg

Subscripts

k	=	design point index
l	=	controller parameter vector index

I. Introduction

IN RECENT years, unmanned aerial vehicles (UAVs) experienced a widespread diffusion and attracted increasing interest for several military as well as civilian applications.

The conventional quad-rotor configuration has the advantage of intrinsic simplicity and reliability and is capable of hovering flight, but suffers from reduced speed, range, and payload capability; on the other hand, the fixed-wing architecture presents complementary advantages and disadvantages. The quad-tilt-wing (QTW) configuration proposes itself as a means to combine the advantages of both: four propellers are mounted to the leading edges of tandem wings, which are capable of tilting from the vertical position (helicopter mode) to the horizontal one (airplane mode); this configuration has recently been receiving increasing attention [1–4]. However, the QTW configuration undergoes significant variations of its aerodynamic characteristics during the conversion process between the two modes, which reflects into a strong dependence of the dynamics of the vehicle on the operating conditions [1]. This consideration, together with uncertainty in the system parameters and in the model, imposes the need for robustness requirements when designing the flight controller.

Japan Aerospace Exploration Agency (JAXA) has been developing different prototypes of UAVs in QTW configuration; see, e.g., the AKITSU [2] and McART3 [5,6] UAVs (see Fig. 1 and Table 1). An attitude control law (namely, stability and control augmentation system, SCAS) was designed (see [2] and references therein for details); the SCAS structure was fixed beforehand, leaving the controller gains as tunable parameters. The design procedure took into account the requirement of robustness, by guaranteeing robust stability and performance against a set containing a finite number of models at the nominal configuration and slightly perturbed configurations; this approach is also referred to as multiple-model approach [7], here also referred to as *parametric*. Gain scheduling of the controller parameters was employed to account for large variations in the dynamics of the system as the configuration changes. Control action moderation was achieved by limiting the search space of the controller gains values in the design stage, in order to prevent actuators saturation and rate saturation. The flight controller was successfully tested in conversion flight in order to demonstrate the potential of the QTW configuration [2,6]. However, a drawback of this design procedure is that the multiple-model approach is based on a necessary robustness condition with respect to the uncertainty that affects the actual system, whereas it is preferable to design SCAS gains based on sufficient conditions.

An alternative approach to QTW-UAV SCAS design, based on the H_∞ framework, is proposed in [8]; this approach takes into account constraints on the controller structure as in [6] and uses particle swarm optimization (PSO) [9] to solve the optimization problem. In this approach, performance requirements are given in the frequency domain and are formalized as weighting functions, and the multiple-model approach is employed as a means to achieve robustness, i.e., again yielding a necessary robustness condition.

This paper focuses on the design of a robust attitude control law for the longitudinal dynamics of the McART3 QTW-UAV, with the objective of improving the existing solution in terms of performance robustness. To tackle the problem, a design procedure based on μ-synthesis is proposed [10]. The resulting controller synthesis problem is a structured μ problem, in that constraints on the structure of both the controller and the scaling for the uncertainties are imposed. Similarly to [8], performance requirements are defined in the frequency domain and encoded in the form of frequency weighting functions. The controller is gain-scheduled: a finite number of design points are defined, the controller is designed at the design points, and the gains are interpolated with respect to the scheduling variable, i.e., wing tilt angle.

Received 13 January 2020; revision received 25 May 2020; accepted for publication 12 July 2020;

*Postdoctoral Research Assistant, Department of Aerospace Science and Technology, via La Masa 34.

†Full Professor, Department of Aerospace Science and Technology, via La Masa 34.

‡Senior Researcher, Flight Research Center, Mitaka.

Fig. 1 JAXA McART3 QTW-UAV prototype.

Table 1 Characteristics of McART3 QTW-UAV

Parameter	Value
Length	1052 mm
Span	1411 mm
Height	432 mm
Gross weight	4.6 kg
Cruise speed	24 m/s
Endurance	10 min
Propellers	12×5.5 in., 2-bladed
Electrical motors	188/277 W

In contrast to the well-known normal multiplicative uncertainty description, we adopt an inverse multiplicative uncertainty description [10], defined at each of the considered design points, to describe the uncertainty of the model. Uncertainty descriptions within H_∞- or μ-control framework are more conservative than the one introduced by the multiple-model approach and provide a sufficient condition for robustness, because they consider an infinite number of models rather than a finite one, thus trying to bridge the gap between the discrete points of the grid of models. Moreover, inverse uncertainty is deemed to be a more suitable tool than other nonparametric descriptions (e.g., the better known multiplicative uncertainty) for describing the uncertainty of the models, because on the one hand inverse uncertainty is capable to describe variations in the number of unstable poles of the plant, and on the other hand it captures uncertainty related to low-frequency dynamics [11]: indeed, the variations of aerodynamic characteristics of QTW have an impact both on the dynamics in the low-frequency range and on the number of unstable poles. The proposed uncertainty description can be effectively employed to obtain a controller that achieves robust performance.

Numerous applications of μ-synthesis to aerospace problems can be found in the literature (see, e.g., [12–22]). In all the cited works, unstructured controller μ-synthesis is employed, except for [22], which considers a structured μ-synthesis problem; in [23] an iterative procedure is proposed where a μ-analysis stage is used to identify worst-case perturbed models, which are then used in a multimodel structured H_∞ synthesis stage. In [24] robust synthesis is carried out by means of the structured H_∞ approach.

In this paper, which follows the work presented in [25], the approach proposed by [26] is implemented; i.e., the structured μ-synthesis problem is reformulated by parameterizing the frequency-dependent scaling matrices and including them among the controller tunable parameters, thus resorting to a structured H_∞ problem that can be solved by means of the nonsmooth optimization techniques described in [27] and implemented in MATLAB. In this approach, the controller gains and the scalings are simultaneously optimized. To show the effectiveness of this synthesis method, a comparison was carried out with another approach to structured μ-synthesis, namely, the $D - K$ iteration approach (see, for instance, [14]). The results show that in some design points the two approaches yield practically identical results, with the simultaneous optimization approach achieving slightly better results in terms of robust performance metric; in other design points, the $D - K$ approach fails in finding a solution comparable to the simultaneous optimization approach. Moreover, the $D - K$ approach requires a remarkably higher computational effort than the simultaneous optimization approach. The results of the comparison are consistent with the findings of previous works by the same authors: a similar comparison can be carried out between the results of [28], where structured H_∞ techniques were applied, and [29], where the $D - K$ iteration approach (to be specific, constant-scaling and controller iteration) was applied to a controller with the same structure. The H_∞ controller was able to resort to similar performance with respect to the controller obtained with $D - K$ iteration, with a smaller computational cost.

Further, another contribution of this paper is the development of a novel tool for worst-case performance robustness analysis: this tool, named *worst-case upper bound*, provides an upper bound to the magnitude of the frequency response of the transfer function of a closed-loop uncertain system, as a function of frequency. This tool can be applied to the single-input–single-output (SISO) case (i.e., in the mixed-sensitivity framework, both the sensitivity function and its associated weighting function are SISO), and can provide an intuitive graphical interpretation of performance robustness, which can be complemented to the Bode magnitude diagram of the nominal closed-loop transfer function.

It should be noticed that the proposed controller design methodology is based on the linear time invariant (LTI) framework; that is, robust stability and performance are guaranteed, for each design point, with respect to a given amount of uncertainty and a certain performance requirement. However, no guarantee on stability and performance is given when considering the transition between the design points, which involves interpolation among the controllers. For this reason, it is necessary to carry out validation on a different model, possibly more accurate than the model(s) used in the design stage. In this work, we validate the design by means of simulations on a nonlinear model of the UAV, in order to verify that stability and performance properties are satisfactory even in the transition between design points. The aim of this paper is to demonstrate that a design procedure based on structured μ-synthesis is not only feasible for the QTW-UAV application, but it is also effective in improving the stability and performance properties of the control system. This work builds upon the results of [2,6] and proposes a different tuning approach, while maintaining the same controller structure.

The paper is organized as follows: Sec. II provides an overview of QTW-UAV with focus on the control system architecture. Section III describes the method to obtain the uncertainty description, and in Sec. IV an overview of stability and performance robustness is provided and the worst-case upper bound tool is introduced. In Sec. V the performance requirements are defined and the synthesis problem is formalized. Finally, in Sec. VI simulation results are shown, carried out both on linearized models of the QTW and on a nonlinear model, and a comparison between different approaches to solve the structured μ-synthesis problem is carried out.

II. Description of QTW

The QTW operates in a range of values of wing tilt angle τ_w from 90 deg (helicopter mode) to 0 deg (airplane mode); furthermore, a so-called CLEAN (i.e., cruise) operating mode at $\tau_w = 0$ deg is defined, with flaps retracted in order to improve efficiency in airplane mode. The set of considered wing tilt angles is the same as in [6]. Wing tilting is not used for control purposes, but rather to set the operating condition of the vehicle like landing gears and conventional flaps. The pilot can manually select the desired wing tilt angle among a discrete set of values. The operating conditions considered in this paper are summarized in Table 2; the operating condition is characterized by the tilt wing angle τ_w. Each operating condition is associated with a trim true airspeed (TAS), which is reported in the table as well.[§]

[§]With a slight abuse of notation, the shorthands defined in Table 2 will be used for convenience in place of the actual values of the tilt wing angle variable τ_w: for instance, the notation $\tau_w = \text{CLEAN}$ will be equivalent to $\tau_w = \tau_{w,12}$ (which is more formally correct).

Table 2 QTW operating points

Variable	Shorthand	τ_w, deg	Trim TAS, m/s
$\tau_{w,1}$	90	90	1.0
$\tau_{w,2}$	80	80	2.5
$\tau_{w,3}$	70	70	5.0
$\tau_{w,4}$	60	60	7.0
$\tau_{w,5}$	50	50	8.0
$\tau_{w,6}$	40	40	9.5
$\tau_{w,7}$	30	30	11.0
$\tau_{w,8}$	20	20	13.0
$\tau_{w,9}$	15	15	14.0
$\tau_{w,10}$	10	10	14.5
$\tau_{w,11}$	0	0	19.0
$\tau_{w,12}$	CLEAN	0	24.0

The operating conditions considered for controller design are listed in Table 3. A number $K = 7$ of design points is considered; let $\mathcal{K} = \{1, \ldots, K\}$ be the set containing the indices related to the design points. For the k th design point, a nominal wing tilt angle $\tau_{wn,k}$, $k \in \mathcal{K}$ is considered and denoted with letter "N" (second column). Additional off-nominal operating conditions are considered at each design point, which can be interpreted as possible modeling errors; let $T_{p,k}$ be the set of perturbed conditions (which are marked as P1 and P2) associated with the kth design point, reported in the third column. Such perturbed models P1 and P2 are set as lower and upper bounds for uncertainty at the specified design point.

Let T_k be the set containing the nominal and perturbed wing tilt angle values associated with the kth design point, defined as

$$T_k = \{\tau_{wn,k}\} \cup T_{p,k} \tag{1}$$

The control architecture of McART3 QTW is very similar to the one described for AKITSU in [2]. Two devices are employed to control longitudinal motion: pitching moment in helicopter mode is provided by differential thrust between forward and aft propellers (referred to as *power elevator*), whereas in airplane mode it is provided by differential deflection of forward and aft flaperons (i.e., *flaperon elevator*), and by a combination of the two in conversion mode. The total thrust is obtained by applying the pilot throttle input to the four propellers.

The model of the longitudinal dynamics is decoupled from the lateral-directional dynamics model: the block diagram of the longitudinal motion SCAS is depicted in Fig. 2. The bare airframe rigid body dynamics, described by states $[u, w, q, \theta]^T$, is denoted in the block diagram as the transfer matrix $G_{\text{lon}}(s; \tau_w)$ and receives as inputs the actuator displacements; the model is linearized in correspondence of the different wing tilt angles τ_w listed in Table 2.

Actuator dynamics are represented as a first-order system for each actuator. The actuator command variables are denoted by the subscript C. Upstream the actuators, the block $K_{\text{lon}}(\tau_w)$ represents the primary flight control system (PFCS; see [2] for details): this is a static gain matrix, which implements the control strategy by allocating the required control action to the actuators based on the operating condition (i.e., it is scheduled as a function of the wing tilt angle τ_w). The input variables to the PFCS are denoted by the subscript CP. The cascade of bare airframe dynamic model, actuators model, and PFCS yields the transfer matrix $G(s; \tau_w)$ from the control inputs $[\delta_{\text{flelv}_{CP}}, \delta_{\text{pwelv}_{CP}}, \delta_{\text{th}_{CP}}]^T$ to the output variables $[q, \theta]^T$ (the state-space models including PFCS and actuators can be found in the Appendix).

The SCAS is composed by a stability augmentation system (SAS) parameterized in the gains $k_{\text{flelv}}(\tau_w)$ and $k_{\text{pwelv}}(\tau_w)$, and by a control augmentation system (CAS) parameterized in $k_{p\theta}(\tau_w)$ and $k_{i\theta}(\tau_w)$. All the aforementioned gains are scheduled as a function of the wing tilt angle τ_w by piecewise linear interpolation among the K design points. The PFCS gains were kept fixed by design; the controller in [6] will be referred to as the baseline controller and the values of its gains are reported in Table 4. In the tuning procedure, SCAS gains are limited by upper and lower bounds, to avoid actuators saturation.

Table 4 SCAS parameter values: baseline controller

Gain	90	70	50	30	15	0	CLEAN
k_{flelv}	0	86	86	86	86	74	57
k_{pwelv}	69	69	69	69	69	0	0
$k_{p\theta}$	−50	−50	−100	−150	−150	−100	−70
$k_{i\theta}$	−40	−40	−70	−100	−100	−100	−33

Table 3 Design points and off-nominal conditions

Design point # k	Nominal condition [shorthand]	Perturbed conditions set [shorthand]
1	$\tau_{wn,1} = \tau_{w,1}[90](N)$	$T_{p,1} = \{\tau_{w,2}[80](P1)\}$
2	$\tau_{wn,2} = \tau_{w,3}[70](N)$	$T_{p,2} = \{\tau_{w,2}[80](P1), \tau_{w,4}[60](P2)\}$
3	$\tau_{wn,3} = \tau_{w,5}[50](N)$	$T_{p,3} = \{\tau_{w,4}[60](P1), \tau_{w,6}[40](P2)\}$
4	$\tau_{wn,4} = \tau_{w,7}[30](N)$	$T_{p,4} = \{\tau_{w,6}[40](P1), \tau_{w,8}[20](P2)\}$
5	$\tau_{wn,5} = \tau_{w,9}[15](N)$	$T_{p,5} = \{\tau_{w,8}[20](P1), \tau_{w,10}[10](P2)\}$
6	$\tau_{wn,6} = \tau_{w,11}[0](N)$	$T_{p,6} = \{\tau_{w,10}[10](P1), \tau_{w,12}[\text{CLEAN}](P2)\}$
7	$\tau_{wn,7} = \tau_{w,12}[\text{CLEAN}](N)$	$T_{p,7} = \{\tau_{w,11}[0](P1)\}$

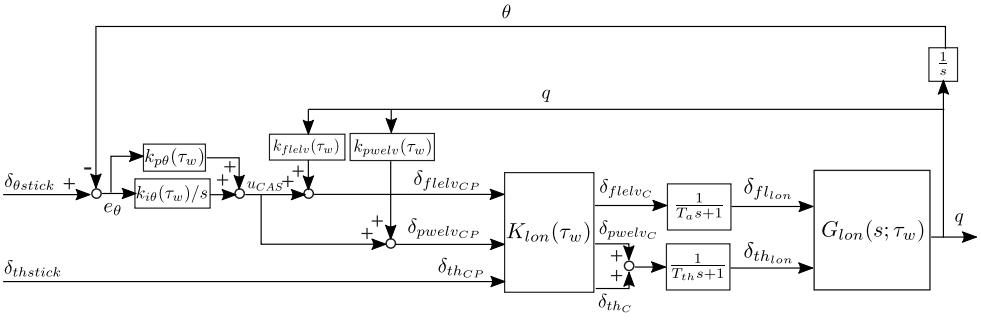

Fig. 2 Longitudinal SCAS block diagram.

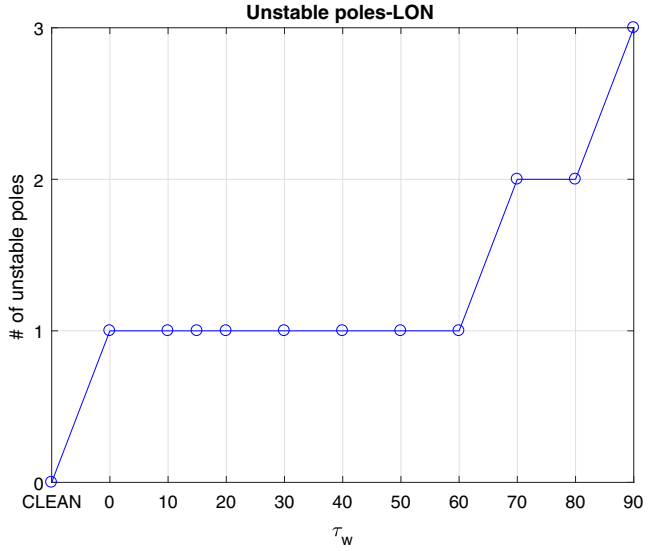

Fig. 3 Number of unstable poles associated with the longitudinal (LON) axis as a function of the operating condition.

The pilot (or the upper layer in the control architecture) has two control inputs, namely, longitudinal stick input $\delta_{\theta\text{stick}}$, which represents the reference pitch angle, and throttle input δ_{thstick}.

Analysis of the poles of the longitudinal models at different operating conditions shows that the number of unstable poles changes as a function of τ_w, with tendency to increased stability when progressing from helicopter to airplane mode (see Fig. 3). Although the theory of LTI modeling and stability analysis is well developed for aircraft in fixed-wing configuration, and it allows to derive analytical, physically motivated expressions of the model dynamics, the same does not hold true for rotorcraft with the capability of tilting wings; especially when considering the transition maneuver, it is not straightforward to derive such analytical expressions of the linearized dynamics about the equilibrium, nor to obtain explicit expressions of the poles of the linearized model as a function of the operating condition or of the physical parameters of the vehicle. As a result, numerical linearization of a nonlinear model of the dynamics about the desired operating condition certainly represents a more feasible way to carry out stability analysis.

III. Uncertainty Description

A nonparametric uncertainty description is employed, based on the set of nominal and perturbed models in Table 3, which allows to describe all possible uncertainties between the perturbed models in the set while minimizing conservatism. This approach requires to define a nominal model and a frequency weighting function that describes the amount of uncertainty as a function of frequency.

An inverse multiplicative uncertainty description (from this point on, also referred to as *inverse uncertainty*) is used [10]. Equation (2) shows the structure of inverse uncertainty description in the case of a generic SISO model in transfer function form:

$$\tilde{F}(s) = (1 + \Delta(s)W_U(s))^{-1}\bar{F}(s) \tag{2}$$

where $\tilde{F}(s)$ is the uncertain model, $\bar{F}(s)$ represents the nominal model, and $W_U(s)$ is the weighting function describing the level of uncertainty as a function of frequency, whereas $\Delta(s)$ is an uncertain transfer function that is bounded as $\|\Delta(j\omega)\| \leq 1\,\forall\,\omega$. The block diagram corresponding to this uncertainty description structure is depicted in Fig. 4.

Given the transfer function of the nominal SISO model $\bar{F}(s)$ and a set Π of perturbed models, and given the transfer function of a perturbed model $F_p(s) \in \Pi$ (or at least its frequency response $F_p(j\omega)$), the inverse uncertainty weighting function $W_U(s)$ is obtained by computing, for each perturbed model, the relative difference with respect to the nominal one:

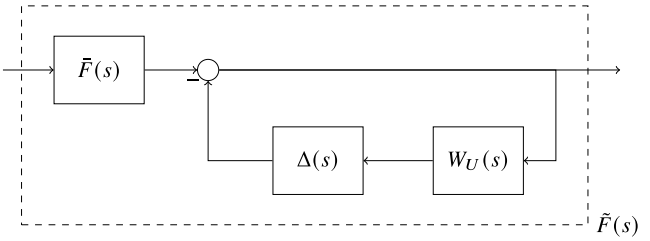

Fig. 4 Inverse multiplicative uncertainty description block diagram.

$$e(\omega) = \frac{\bar{F}(j\omega) - F_p(j\omega)}{F_p(j\omega)} \tag{3}$$

and by upper-bounding the worst-case error over the entire set of perturbed models one obtains:

$$l(\omega) = \max_{F_p \in \Pi} \left| \frac{\bar{F}(j\omega) - F_p(j\omega)}{F_p(j\omega)} \right| \tag{4}$$

The computation is carried out frequency by frequency, following the approach described in [10] for the multiplicative uncertainty case. The nonparametric worst-case error is then approximated by the frequency response magnitude of a rational, proper, stable, minimum phase transfer function $W_U(s)$ by means of a fitting routine, such that $|W_U(j\omega)| \geq l(\omega)\,\forall\,\omega$.

The rationale behind the choice of inverse multiplicative uncertainty was stated in the Introduction. One of the reasons is that, as was discussed in Sec. II, the number of unstable poles of the QTW model changes with the wing tilt angle.

Based on the notation introduced in Sec. II, the nominal model associated with the k th design point is defined as

$$\bar{G}_k(s) = G(s; \tau_{wn,k}) \qquad \forall\ k \in \mathcal{K} \tag{5}$$

The formulation of the uncertainty description related to the longitudinal model will be discussed hereafter: no coupling with other axes is involved in the feedback, thus allowing to obtain a SISO uncertainty description.

Let $G_q(s)$ be the transfer function from the input variables $[\delta_{\text{flelv}_{CP}}, \delta_{\text{pwelv}_{CP}}]^T$ to the output q; let $G_{\text{th}}(s)$ be the transfer function from the input $\delta_{\text{th}_{CP}}$ to the output q.

An analysis of the longitudinal SCAS architecture shows that the variables involved in the feedback are output variables q and θ, and input variables $\delta_{\text{flelv}_{CP}}$ and $\delta_{\text{pwelv}_{CP}}$.

The input variable $\delta_{\text{th}_{CP}}$ is not involved in feedback in that, because the pilot is commanding attitude (with SAS as well as CAS engaged), the pilot throttle command δ_{thstick} is directly fed to $\delta_{\text{th}_{CP}}$ (see Fig. 2); that is, $\delta_{\text{th}_{CP}}$ can be considered an exogenous input variable. Hence, $\delta_{\text{th}_{CP}}$ can be discarded from the list of input variables in the computation of the uncertainty description, because it does not affect stability of the closed-loop system. Indeed, the focus is to obtain an uncertain model that can be used to assess robustness of the stability and performance properties associated with the attitude control loop. Under these assumptions, $G_{\text{th}}(s)$ is considered to be unaffected by uncertainty to simplify the procedure.

As for the output variables, since $\theta \simeq (1/s)q$ for small displacements about wing-level flight, the pitch angle can be discarded from the list of output variables as well, and can be reintroduced later by integrating the angular rate output variable of the uncertain model.

One could then consider the (SISO) open-loop transfer function $G_q^S(s)$ from the CAS output u_{CAS} to q (see again Fig. 2):

$$G_q^S(s) = G_q(s)M = \frac{q}{u_{\text{CAS}}} \tag{6}$$

where

$$q = G_q(s)\begin{bmatrix}\delta_{\text{flelv}_{CP}}\\ \delta_{\text{pwelv}_{CP}}\end{bmatrix}, \qquad M = \begin{bmatrix}1\\1\end{bmatrix} \tag{7}$$

Note that the commands for $\delta_{\text{flelv}_{CP}}$ and $\delta_{\text{pwelv}_{CP}}$ are the same; however, PFCS reflects the efficiency of these control devices. Thus, the actual inputs to flaperons and throttle are not equivalent. The procedure to obtain the nonparametric uncertain model is then outlined as follows, and is applied to each of the design points in Table 3:

1) Pick the kth design point, with nominal model $\bar{G}_k(s)$ and the models associated with the corresponding set of perturbed operating conditions $T_{p,k}$.

2) Define the transfer functions from the control inputs $[\delta_{\text{flelv}_{CP}}, \delta_{\text{pwelv}_{CP}}]^T$ to the output q in the nominal and perturbed cases, respectively, as $\bar{G}_{q,k}(s)$ and $G_q(s;\tau_w)$, $\tau_w \in T_{p,k}$; define the nominal transfer function from $\delta_{\text{th}_{CP}}$ to q as $\bar{G}_{\text{th},k}(s)$.

3) Compute the SISO transfer function as from Eq. (6), for the nominal and perturbed models, obtaining, respectively, $\bar{G}^S_{q,k}(s)$ and $G^S_q(s;\tau_w)$, $\tau_w \in T_{p,k}$.

4) Compute the worst-case relative error between the nominal model $\bar{G}^S_{q,k}(j\omega)$ and the perturbed models $G^S_q(j\omega;\tau_w)$, $\tau_w \in T_{p,k}$ as defined in Eq. (4):

$$l_k(\omega) = \max_{\tau_w \in T_{p,k}} \left| \frac{\bar{G}^S_{q,k}(j\omega) - G^S_q(j\omega;\tau_w)}{G^S_q(j\omega;\tau_w)} \right| \tag{8}$$

5) Obtain the nonparametric uncertainty description $W_{U,k}(s)$ by upper-bounding $l_k(\omega)$ with a magnitude fitting routine.

6) Define the nonparametric uncertain model as

$$\begin{bmatrix}q\\ \theta\end{bmatrix} = \tilde{G}_k(s)\begin{bmatrix}\delta_{\text{flelv}_{CP}}\\ \delta_{\text{pwelv}_{Cp}}\\ \delta_{\text{th}_{CP}}\end{bmatrix} \tag{9}$$

where

$$\tilde{G}_k(s) = \begin{bmatrix}1\\ \frac{1}{s}\end{bmatrix}\begin{bmatrix}\tilde{G}_{q,k}(s) & \bar{G}_{\text{th},k}(s)\end{bmatrix} \tag{10}$$

$$\tilde{G}_{q,k}(s) = (1 + \Delta(s)W_{U,k}(s))^{-1}\bar{G}_{q,k}(s) \tag{11}$$

$$\|\Delta(s)\|_\infty \le 1 \tag{12}$$

Table 5 summarizes the input and output variables and the dimensions of the transfer functions involved in the computation of the uncertainty description weighting function. In particular, $\tilde{G}_k(s)$ indicates the uncertain version of the model $G(s)$ at the design point k, so it has the same input–output interface as $G(s)$. When building the expression of the uncertain plant $\tilde{G}_k(s)$ in Eq. (10), two components are stacked together: an uncertain part (i.e., $\tilde{G}_{q,k}(s)$, which represents the part of the system related to inputs $[\delta_{\text{flelv}_{CP}}, \delta_{\text{pwelv}_{CP}}]^T$ and output q; see Eq. (11), and a nominal part that is unaffected by uncertainty (i.e., $\bar{G}_{\text{th},k}(s)$, the part of the system related to input $\delta_{\text{th}_{CP}}$). Also, in Eq. (10) it can be noticed that an integrator $(1/s)$ appears: with this procedure θ is recovered as an output variable, by integrating q downstream the uncertainty in the model.

Table 5 Uncertainty computation: dimensions and input/output variables of transfer functions

Transfer function	Inputs	Outputs	Dimensions
$G(s), \bar{G}_k(s), \tilde{G}_k(s)$	$[\delta_{\text{flelv}_{CP}}, \delta_{\text{pwelv}_{CP}}, \delta_{\text{th}_{CP}}]^T$	$[q, \theta]^T$	$[2 \times 3]$
$G_q(s), \bar{G}_{q,k}(s), \tilde{G}_{q,k}(s)$	$[\delta_{\text{flelv}_{CP}}, \delta_{\text{pwelv}_{CP}}]^T$	q	$[1 \times 2]$
$G_{\text{th}}(s), \bar{G}_{\text{th},k}(s)$	$\delta_{\text{th}_{CP}}$	q	$[1 \times 1]$
$G^S_q(s), \bar{G}^S_{q,k}(s)$	u_{CAS}	q	$[1 \times 1]$

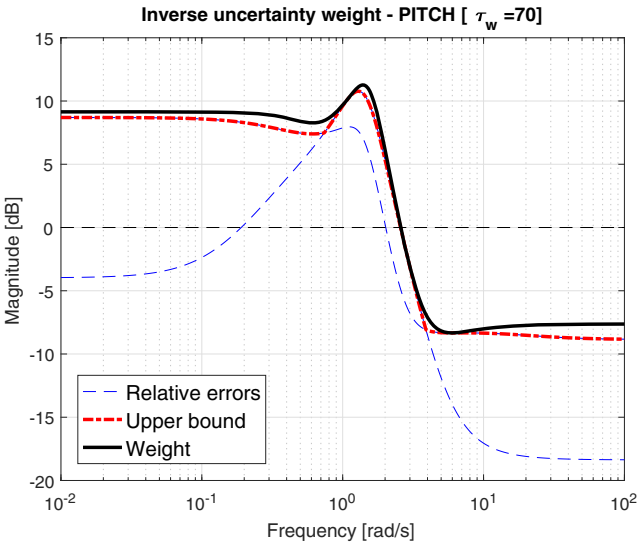

Fig. 5 Inverse multiplicative uncertainty weight, $\tau_w = 70$ design point.

The weighting functions were chosen as stable, nonstrictly proper transfer functions of order 4, which led to a satisfactory fitting of the magnitude of relative errors. As an example, the inverse uncertainty weighting function obtained for the design point $\tau_w = 70$ is shown in Fig. 5.

IV. Performance Robustness and the Worst-Case Upper Bound

In this section, a brief overview on conditions to determine robustness of properties such as stability and performance of a closed-loop system with respect to model uncertainty is given. Uncertainty can be represented in a parametric (i.e., multiple-model) form, such as the one formalized in Table 3, or in a nonparametric form, such as the uncertain model developed in Sec. III; in this case, the nonparametric uncertainty description is built based on its parametric counterpart and is more conservative with respect to it. A more complete treatment of this topic can be found in [10]; as for the worst-case analysis paragraph, the reader is referred to [30] for a more detailed discussion.

As stated in the Introduction, it is remarked that the robustness framework considered in this work is based on LTI modeling; that is, the tools for robustness analysis and synthesis here presented are valid when considering a specific design point, but no guarantees on stability and performance robustness hold when considering the transition between design points.

A. Robustness Conditions in the Nonparametric Case

The following analysis is carried out within the linear fractional transformation (LFT) framework. An uncertain closed-loop system with nonparametric uncertainty structure can be rearranged as the feedback interconnection of an augmented plant $P(s)$, the controller $K(s)$, and an uncertain block $\Delta(s)$ that is bounded in magnitude and can possess structure (see Fig. 6). The augmented plant $P(s)$ depends on the nominal model of the system, the performance requirements stated in the form of a frequency weighting function (as will be described in Sec. V.A), and the nonparametric uncertainty description obtained as explained in Sec. III.

Define $F_l(P(s), K(s))$ as the lower LFT interconnection of $P(s)$ and $K(s)$, and $F_u(P(s), \Delta(s))$ as the upper LFT interconnection of $P(s)$ and $\Delta(s)$. Loop closure on the controller $K(s)$ yields (by means of a lower LFT):

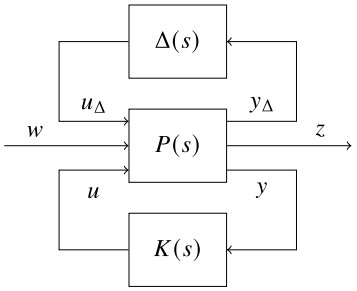

Fig. 6 LFT connection of P, Δ, and K.

$$N(s) = F_l(P(s), K(s)) = \begin{bmatrix} N_{11}(s) & N_{12}(s) \\ N_{21}(s) & N_{22}(s) \end{bmatrix} \tag{13}$$

where the four blocks of Eq. (13) reflect the input–output interface of $N(s)$:

$$\begin{bmatrix} y_\Delta \\ z \end{bmatrix} = N(s) \begin{bmatrix} u_\Delta \\ w \end{bmatrix} \tag{14}$$

The controller $K(s)$ stabilizes $N(s)$. The nominal stability (NS) of the closed-loop system (i.e., no uncertainty, which is equivalent to neglecting the feedback loop on Δ) can be studied looking at the poles λ of $N(s)$:

$$\text{NS} \Leftrightarrow \max_{\lambda} \text{Re}(\lambda) < 0 \tag{15}$$

Similarly, nominal performance (NP) can be studied by looking at the part of the closed-loop system transfer function related to the input–output performance channel, i.e., $N_{22}(s)$:

$$\text{NP} \Leftrightarrow \max_{\omega} \bar{\sigma}(N_{22}(j\omega)) < 1 \tag{16}$$

In the nonparametric case, robust stability (RS) can be assessed by checking a condition on the frequency response function of $N_{11}(s)$:

$$\text{RS} \Leftrightarrow \max_{\omega} \mu_\Delta(N_{11}(j\omega)) < 1 \tag{17}$$

where μ_Δ is the structured singular value operator applied to a perturbation with structure consistent with the Δ block. The μ_Δ operator, in the case $\Delta(s)$ is an unstructured full-block perturbation (e.g., it is a full complex matrix), can be replaced by

$$\mu_\Delta(N_{11}(j\omega)) = \bar{\sigma}(N_{11}(j\omega)) \tag{18}$$

so that the robust stability condition simplifies to

$$\text{RS} \Leftrightarrow \max_{\omega} \bar{\sigma}(N_{11}(j\omega)) < 1 \tag{19}$$

Robust performance (RP) analysis can be carried out by defining a fictitious uncertain full block $\Delta_P(s)$ compatible with the dimensions of the performance input and output signals. Define the structured augmented uncertain block $\hat{\Delta}(s)$ as

$$\hat{\Delta}(s) = \begin{bmatrix} \Delta(s) & 0 \\ 0 & \Delta_P(s) \end{bmatrix} \tag{20}$$

The robust performance condition is

$$\text{RP} \Leftrightarrow \max_{\omega} \mu_{\hat{\Delta}}(N(j\omega)) < 1 \tag{21}$$

B. Robustness Conditions in the Multiple-Model Case

The robustness analysis of uncertain closed-loop systems defined according to the multiple-model (i.e., parametric uncertainty) paradigm can be formulated in the LFT framework described in the previous section.

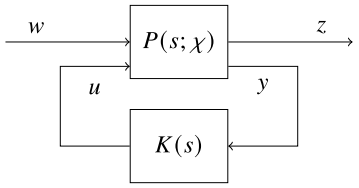

Fig. 7 LFT connection of P and K.

In this case, the model of the plant $G(s;\chi)$ depends on a parameter $\chi \in X$, where the set X is of finite dimension. The nominal model $\bar{G}(s) = G(s;\chi_n)$ corresponds to the nominal parameter value $\chi_n \in X$.

In a similar way as described in the previous section, an augmented plant model of the system can be defined as $P(s;\chi)$: in this case, the augmented plant depends on the model $G(s;\chi)$ (which in turn depends on the parameter χ) and on the performance requirements. The main differences with respect to the nonparametric case are as follows:

1) There is one augmented plant $P(s;\chi)$ for each of the values of $\chi \in X$, whereas in the nonparametric case there is only one augmented plant $P(s)$.

2) Whereas in the nonparametric case the augmented plant depends on the (nonparametric) uncertainty description, in this case there is simply no explicit uncertainty description, but the uncertainty implicitly comes from the fact that perturbed models of the system are considered.

The augmented plant is closed in loop with the controller $K(s)$ by means of the lower LFT operator (see the block diagram in Fig. 7; notice that the controller does not depend on χ but it is the same for all plants):

$$N(s;\chi) = F_l(P(s;\chi), K(s)) \tag{22}$$

where, unlike Eq. (13), in which $N(s)$ is decomposed into four blocks, in this case $N(s;\chi)$ has w and z as input and output signals, respectively.

Nominal stability for the multiple-model case (NS_{MM}) is guaranteed if the poles $\lambda(N(s;\chi_n))$ of the augmented plant corresponding to the nominal model meet the following condition:

$$\text{NS}_{\text{MM}} \Leftrightarrow \max_{\lambda} \text{Re}(\lambda) < 0 \tag{23}$$

Nominal performance (NP_{MM}), similarly, can be studied by means of the nominal closed-loop augmented plant $N(s;\chi_n)$:

$$\text{NP}_{\text{MM}} \Leftrightarrow \max_{\omega} \bar{\sigma}(N(j\omega;\chi_n)) < 1 \tag{24}$$

Robust stability (RS_{MM}) is achieved if the nominal stability condition holds when applied to the system closed in loop with any of the perturbed models:

$$\text{RS}_{\text{MM}} \Leftrightarrow \max_{\chi \in X} \max_{\lambda} \text{Re}(\lambda) < 0 \tag{25}$$

where $\lambda(N(s;\chi)), \chi \in X$ this time represents the poles of the closed-loop system at the parameter χ.

Similarly, robust performance (RP_{MM}) is achieved if the nominal performance condition holds true even when applied to any of the closed-loop perturbed models $N(s;\chi), \chi \in X$:

$$\text{RP}_{\text{MM}} \Leftrightarrow \max_{\chi \in X} \max_{\omega} \bar{\sigma}(N(j\omega;\chi)) < 1 \tag{26}$$

C. Worst-Case Analysis

Another metric for characterizing robust performance in the nonparametric framework is the worst-case performance. Robust performance can be stated as

$$\max_{\Delta} \bar{\sigma}(F_u(N(j\omega), \Delta(j\omega))) < 1 \qquad \forall\ \omega \tag{27}$$

where $F_u(N(s), \Delta(s))$ is the upper-LFT interconnection between the augmented nominal closed-loop system $N(s)$ and the uncertain block $\Delta(s)$ (which may possess structure). The condition in Eq. (27) can be interpreted as follows: the uncertain closed-loop transfer function from performance input w to performance output z shall meet the performance requirement for any value of $\Delta(s)$, at all frequencies. Worst-case analysis is about finding the largest peak of the perturbed closed-loop transfer function:

$$p_{\text{wc}} \triangleq \max_{\omega} \max_{\Delta} \bar{\sigma}(F_u(N(j\omega), \Delta(j\omega))) \tag{28}$$

The frequency at which the peak is attained is defined as follows:

$$\omega_{\text{wc}} \triangleq \arg\max_{\omega} \max_{\Delta} \bar{\sigma}(F_u(N(j\omega), \Delta(j\omega))) \tag{29}$$

Let the skewed structured singular value (μ^s or skewed-μ) be defined as follows (see [10] for a thorough treatise of skewed-μ and its properties):

$$\mu^s(N(j\omega)) = \frac{1}{\min\{k_m | \det(I - K_m N(j\omega)\Delta) = 0\}} \tag{30}$$

$$K_m = \begin{bmatrix} I & 0 \\ 0 & k_m I \end{bmatrix} \tag{31}$$

for some allowed Δ of prescribed structure such that $\bar{\sigma}(\Delta) \leq 1$, where K_m is a scaling matrix depending on k_m, defining which of the uncertain sub-blocks of Δ are to be scaled, whereas the other ones will remain of fixed size.

Worst-case performance is characterized by μ^s, which can be used to compute the worst-case performance index p_{wc} defined in Eq. (28):

$$\max_{\Delta} \bar{\sigma}(F_u(N(j\omega), \Delta(j\omega))) = \mu^s(N(j\omega)) \tag{32}$$

$$p_{\text{wc}} = \max_{\omega} \mu^s(N(j\omega)) \tag{33}$$

$$\omega_{\text{wc}} = \arg\max_{\omega} \mu^s(N(j\omega)) \tag{34}$$

Skewed-μ is applied to the uncertainty structure $\hat{\Delta}(s)$ defined in Eq. (20): it allows to keep the amount of uncertainty Δ bounded ($\bar{\sigma}(\Delta) \leq 1$) and to vary the amount of uncertainty Δ_P related to the performance requirement. In this sense, skewed-μ represents a generalization of the structured singular value. For a thorough discussion on skewed-μ and worst-case performance analysis, the reader is referred to [10] (see in particular Chapter 8.10).

D. Worst-Case Upper Bound

In the particular case the closed-loop transfer function associated with the performance requirement is SISO (and the performance weighting function is SISO as well); it is possible to provide a graphical representation of the worst-case magnitude of the closed-loop transfer function. Suppose that

$$F_u(N(s), \Delta(s)) = W_S(s) S(s, \Delta(s)) \tag{35}$$

where $W_S(s)$ is the performance weighting function and $S(s, \Delta(s))$ is the closed-loop perturbed transfer function related to performance. Equation (32) can be rewritten as

$$|W_S(j\omega)| \max_{\Delta} |S(j\omega, \Delta(j\omega))| = \mu^s(N(j\omega)) \tag{36}$$

thus

$$|S(j\omega, \Delta(j\omega))| \leq \max_{\Delta} |S(j\omega, \Delta)| = \frac{\mu^s(N(j\omega))}{|W_S(j\omega)|} \tag{37}$$

The right-hand term in Eq. (37) provides for each frequency an upper bound to the magnitude of the perturbed closed-loop transfer function $S(s, \Delta(s))$. This quantity is defined as the worst-case upper bound and is defined as follows:

$$S_{\text{WC}}(\omega) \triangleq \frac{\mu^s(N(j\omega))}{|W_S(j\omega)|} \tag{38}$$

V. Structured μ-Synthesis for McART3 QTW Longitudinal Control

A. Performance Characterization

Performance is characterized in the frequency domain by the sensitivity function $S_\theta(s)$ obtained by breaking the loop in the pitch attitude tracking error signal e_θ; a weighting function $W_S(s)$ is used to encode performance requirements in the frequency domain. The H_∞ norm of the weighted sensitivity function provides a performance metric:

$$\|W_S(s) S_\theta(s)\|_\infty \tag{39}$$

More in detail, performance can be quantified by means of two parameters defined in [31]: the disturbance rejection bandwidth (DRB, i.e., the bandwidth of the sensitivity function), and the disturbance rejection peak (DRP, i.e., the magnitude peak over frequency of the sensitivity function).

Following the notation of the previous sections, consider the nominal model $\bar{G}_k(s)$ and the set T_k containing the nominal and perturbed operating conditions associated with the k th design point; let $K_k(s)$ be the controller computed in the same design point. Let $W_{S,k}(s)$ be the weighting function that encodes the performance requirement associated with the k th design point.

Let $\bar{S}_{\theta,k}(s)$ be the nominal sensitivity function (extracted from the multiple-input–multiple-output, MIMO, sensitivity $\bar{S}_k(s) = (I + \bar{G}_k(s)K_k(s))^{-1}$), and let $S_{\theta,k}(s; \tau_w)$ be the perturbed pitch sensitivity function related to model $G(s; \tau_w)$, extracted from $S_k(s; \tau_w) = (I + G(s; \tau_w)K_k(s))^{-1}$, $\tau_w \in T_k$.

The nominal performance requirement is expressed in terms of the metric defined in Eq. (39):

$$\|W_{S,k}(s) \bar{S}_{\theta,k}(s)\|_\infty < 1 \tag{40}$$

The performance encoded as the weighting function $W_{S,k}(s)$ is robustly achieved in the presence of uncertainty, in the parametric sense, if the performance requirement is satisfied not only for the nominal condition but also for all the perturbed conditions associated with that particular design point:

$$\max_{\tau_w \in T_k} \|W_{S,k}(s) S_{\theta,k}(s; \tau_w)\|_\infty < 1 \tag{41}$$

B. Requirements Definition

The performance requirements to be used in the synthesis of the control law are defined as follows:

1) A set of so-called original performance level, referred to as WP0, is compatible with the performance achieved by the baseline controller in [6].

2) A set of more aggressive performance requirements, referred to as WP1, is meant to be used to improve longitudinal performance compared with the baseline solution.

The performance requirement set WP0 was defined based on the robust performance level (to be meant in the parametric sense) achieved by the baseline SCAS. One different weighting function $W_{S,k}(s)$, $k \in \mathcal{K}$ was defined for each of the design points defined in Table 3. A parametric approach was employed to define the frequency weighting

Table 6 WP0 performance requirements weighting functions parameters

Design point τ_w	K_{DC}	K_{HF}	z	p	DRB, rad/s	DRP, dB
CLEAN	89	0.815	0.6997	0.0064	0.497	1.8
0	66	0.299	1.2487	0.0057	0.271	10.5
15	100	0.393	0.1588	0.0006	0.046	8.1
30	100	0.393	0.1588	0.0006	0.046	8.1
50	100	0.155	0.0811	0.0001	0.009	16.2
70	60	0.338	0.8780	0.0050	0.217	9.4

Table 7 WP1 performance requirements weighting functions parameters

Design point τ_w	K_{DC}	K_{HF}	z	p	DRB, rad/s	DRP, dB
CLEAN	100	0.800	0.8732	0.0070	0.6	1.9
0	100	0.700	0.5259	0.0037	0.3	3.1
15	100	0.800	0.4366	0.0035	0.3	1.9
30	100	0.700	0.5259	0.0037	0.3	3.1
50	100	0.700	0.5259	0.0037	0.3	3.1
70	100	0.473	0.8440	0.0040	0.3	6.5

functions: that is, for each of the design points, the frequency weighting function $W_{S,k}(s)$ is chosen so that the inverse of the weight magnitude tightly covers the worst-case performance, i.e., the upper envelope of the magnitude of the sensitivity function in nominal and perturbed conditions $S_{\theta,k}(s;\tau_w), \tau_w \in T_k$. The performance requirement weighting function was chosen as a stable transfer function and was parameterized as $W_S(s) = K_{HF}(s+z)/(s+p)$. Parameters of the weighting function for the different design points are reported in Table 6, together with the corresponding values of DC-gain (K_{DC}), DRB, and DRP.

The set of more aggressive performance weights WP1 was chosen based on a trial-and-error procedure in which weights were progressively tightened until eventually achieving robust performance in the synthesis stage. Parameters are reported in Table 7. As an example, the original and aggressive performance weights for the design point $\tau_w = 15$ are represented in Fig. 8 by the inverse of the magnitude of their frequency responses; the sensitivity weight for the aggressive requirement features wider DRB and lower DRP.

As for the admissible values for the controller parameters, two sets of bounds on controller gains were considered:

1) First are the original bounds considered in [6], referred to as BND0 and reported in Table 8.

2) Second is a new set of bounds, obtained by multiplying by a factor two the upper bounds of positive parameters and the lower

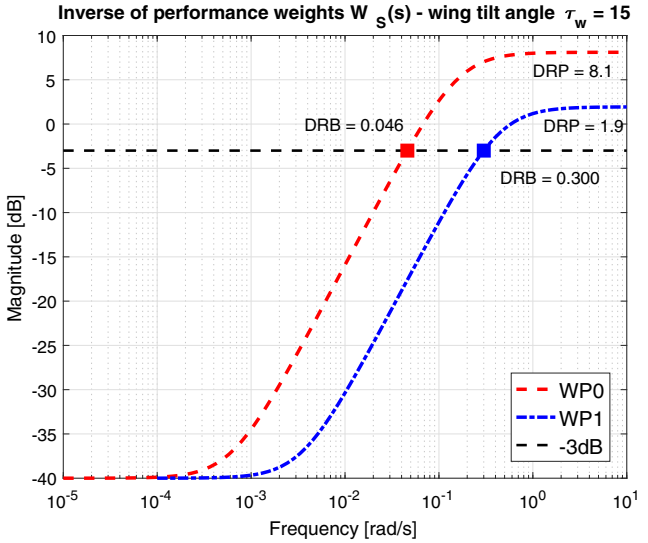

Fig. 8 Inverse of performance requirements weights, design point $\tau_w = 15$.

Table 8 Bounds on SCAS gains: BND0 (first row: minimum value, second row: maximum value)

Gain	Unit	90	70	50	30	15	0	CLEAN
k_{flelv}	%/(rad/s)	0	0	0	0	0	0	0
		0	86	86	86	86	74	57
k_{pwelv}	%/(rad/s)	0	0	0	0	0	0	0
		69	69	69	69	69	0	0
$k_{p\theta}$	%/rad	−50	−50	−100	−150	−150	−100	−70
		0	0	0	0	0	0	0
$k_{i\theta}$	%/(rad · s)	−40	−40	−70	−100	−100	−100	−70
		0	0	0	0	0	0	0

Table 9 Combinations of bounds set and performance requirements set used in μ-synthesis

	BND0	BND1
WP0	*A*	— —
WP1	*B*	*C*

bounds of negative parameters in the original set of bounds; such set of relaxed bounds is referred to as BND1. Under the assumption that an accurate model of the actuators is available, it would be acceptable to relax the bounds.

The second bounds are set to examine control performance improvement by relaxing the original bounds.

To show the effectiveness of the proposed design method, three controllers were obtained, by imposing different combinations of performance requirements and gain bounds in control law synthesis:

1) A controller denoted as *A* is obtained by imposing original performance requirements WP0 and original gain bounds BND0 in the synthesis stage; this controller is expected to meet a performance level comparable to the baseline controller, while guaranteeing robustness with respect to the modeled nonparametric uncertainty.

2) A controller denoted as *B* is obtained by imposing aggressive performance requirements WP1 and original gain bounds BND0, thus representing a more ambitious design challenge with respect to controller *A*.

3) A controller denoted as *C* is obtained by imposing aggressive performance requirements WP1 and relaxed gain bounds BND1.

The mapping of controllers to requirements is summarized in Table 9.

C. Synthesis Problem Setup

Consider the synthesis problem at the k th design point, $k \in \mathcal{K}$. Let $P_k(s)$ be the plant augmented with the uncertainty and performance weights, respectively, $W_{U,k}(s)$ and $W_{S,k}(s)$:

$$P_k(s) = \begin{bmatrix} -W_{U,k}(s) & 0 & W_{U,k}(s)\bar{G}_{q,k}(s) \\ \frac{1}{s}W_{S,k}(s) & W_{S,k}(s) & -\frac{1}{s}W_{S,k}(s)\bar{G}_{q,k}(s) \\ -\frac{1}{s} & 0 & \frac{1}{s}\bar{G}_{q,k}(s) \\ -1 & 0 & \bar{G}_{q,k}(s) \end{bmatrix} \tag{42}$$

The expression of the augmented plant in Eq. (42) can be reconstructed based on the following relationships, consistently with the block diagram depicted in Fig. 9:

$$\begin{bmatrix} y_\Delta \\ z \\ \theta \\ q \end{bmatrix} = P_k(s) \begin{bmatrix} u_\Delta \\ w \\ u \end{bmatrix} \tag{43}$$

$$q = \bar{G}_{q,k}(s)u - u_\Delta \tag{44}$$

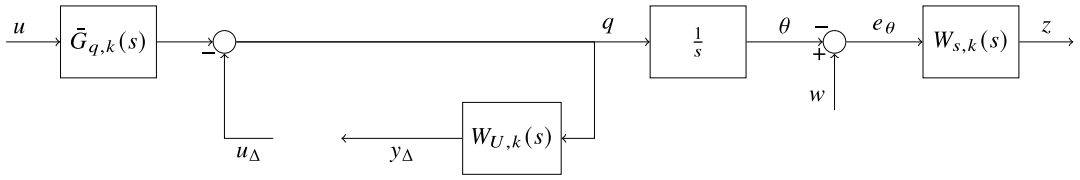

Fig. 9 Augmented plant block diagram.

$$y_\Delta = W_{U,k}(s)q = W_{U,k}(s)\bar{G}_{q,k}(s)u - W_{U,k}(s)u_\Delta \tag{45}$$

$$\theta = \frac{1}{s}q \tag{46}$$

$$e_\theta = w - \theta \tag{47}$$

$$z = W_{S,k}(s)e_\theta = W_{S,k}(s)w - W_{S,k}(s)\theta \tag{48}$$

where

$$u = K_k(s;\rho)y, \quad y = \begin{bmatrix}\theta\\ q\end{bmatrix}, \qquad u = \begin{bmatrix}\delta_{\text{flelv}_{\text{CP}}}\\ \delta_{\text{pwelv}_{\text{CP}}}\end{bmatrix} \tag{49}$$

$$u_\Delta = \Delta(s)y_\Delta, \qquad \|\Delta(s)\|_\infty \le 1 \tag{50}$$

Let $K_k(s;\rho)$ be the structured controller depending on a vector of tunable parameters $\rho \in \mathbb{R}^{n_\rho}$, subject to bounds $\underline{\rho}_k, \bar{\rho}_k$ on their admissible values. The lower-LFT feedback interconnection $F_l(\cdot)$ of $P_k(s)$ and $K_k(s;\rho)$ yields

$$N_k(s;\rho) = F_l(P_k(s), K_k(s;\rho)) = \begin{bmatrix}N_{k,11}(s;\rho) & N_{k,12}(s;\rho)\\ N_{k,21}(s;\rho) & N_{k,22}(s;\rho)\end{bmatrix} \tag{51}$$

The problem of synthesizing a controller achieving robust performance is a structured μ problem, in that it involves constraints on the structure of both K and $\hat{\Delta}$, and can be formalized as

$$\min_\rho \max_\omega \mu_{\hat{\Delta}}(N_k(j\omega;\rho)) \tag{52}$$

subject to

$$\underline{\rho}_{k,l} \le \rho_l \le \bar{\rho}_{k,l} \quad l = 1,\dots,n_\rho \tag{53}$$

According to the approach proposed by [26], the μ-synthesis problem can be reformulated as a structured H_∞ problem on the scaled plant

$$\tilde{N}_k(s;\tilde{\rho}) = D_k(s;\rho_s)N_k(s;\rho)D_k(s;\rho_s)^{-1} \tag{54}$$

where the scaling $D_k(s;\rho_s)$ depends on frequency and has been parameterized in $\rho_s \in \mathbb{R}^{n_s}$, and its structure is compatible with the uncertainty structure $\hat{\Delta}$. Having defined $\tilde{\rho} = [\rho^T, \rho_s^T]^T \in \mathbb{R}^{n_\rho+n_s}$ as the augmented tunable parameters vector, containing controller and scaling parameters, the resulting structured H_∞ problem is

$$\min_{\tilde{\rho}} \|\tilde{N}_k(s;\tilde{\rho})\|_\infty \tag{55}$$

subject to

$$\underline{\rho}_{k,l} \le \rho_l \le \bar{\rho}_{k,l} \quad l = 1,\dots,n_\rho \tag{56}$$

The optimal augmented parameter vector for the k th design point is

$$\tilde{\rho}_k^* = \arg\min_{\tilde{\rho}} \|\tilde{N}_k(s;\tilde{\rho})\|_\infty \tag{57}$$

$$= [(\rho_k^*)^T, (\rho_{s,k}^*)^T]^T \tag{58}$$

where the optimal controller parameter vector is ρ_k^*.

It is remarked that in this approach to structured-μ controller synthesis the parameters ρ_s of the scaling $D_k(s;\rho_s)$ are tuned simultaneously with the controller gains ρ.

D. Comparison with Previous Results

As a conclusion to this section, a brief comparison between the approach employed to carry out the baseline solution, obtained in [6], and the approach proposed in this paper is outlined in the following and summarized in Table 10:

1) *Uncertainty description:* The baseline controller was obtained considering a parametric uncertainty description, i.e., a nominal model and a finite number of perturbed models, and synthesis is carried out according to the multiple-model paradigm. The proposed approach is based on a nonparametric uncertainty description (i.e., an infinite number of perturbed models) and on structured μ-synthesis. As a consequence, the respective robustness criteria yield a necessary condition to robustness in the former case, and a sufficient condition in the latter one.

2) *Performance metric:* The baseline controller was obtained by minimizing a time-domain-based performance cost function related to tracking error; on the other hand, the proposed approach defines a frequency-domain-based cost function.

3) *Optimization method:* The baseline controller was designed directly searching the optimal cost function value on a grid of the controller parameter space; the proposed approach is based on nonsmooth optimization techniques. Moreover, in the baseline approach, SAS and CAS gains were optimized in subsequent steps, whereas in the proposed approach all gains are optimized simultaneously.

VI. Simulation Results

A. Numerical Results

The optimization was run by means of the MATLAB systune function; optimal values of the longitudinal SCAS parameters $\rho = [k_{p\theta}, k_{i\theta}, k_{\text{pwelv}}, k_{\text{flelv}}]^T$ were found for all the design points in Table 3, except for the condition $\tau_w = 90$, because, as it was already pointed out in [2,6], it was not possible to stabilize the closed-loop system in this condition with attitude angle and rate feedback only; though, it was verified that the unstable modes with SAS in [6] are slow enough to be manually stabilized by a human pilot.

Table 10 Comparison of QTW-UAV SCAS design methods

Feature	Baseline	μ-synthesis
Uncertainty description	Parametric (multiple-model)	Nonparametric (inverse multiplicative)
Robustness condition	Necessary	Sufficient
Performance metric	Time domain	Frequency domain
Optimization method	Direct search on grid	Nonsmooth, nonconvex optimization (MATLAB systune)
Tuning strategy	SAS and CAS are optimized sequentially	SAS and CAS are optimized simultaneously

The three controllers A, B, and C, characterized by the requirements outlined in Table 9, were tuned; gain values are reported, respectively, in Tables 11–13.

Consistently with Sec. IV, three cost functions, to be evaluated on the augmented closed-loop system as metrics for verification of robust stability (RS), nominal performance (NP), and robust performance (RP), are defined as follows:

$$J_{\mathrm{RS}} = \|N_{11}(s)\|_\infty = \max_\omega \bar{\sigma}(N_{11}(j\omega)) \tag{59}$$

$$J_{\mathrm{NP}} = \|N_{22}(s)\|_\infty = \max_\omega \bar{\sigma}(N_{22}(j\omega)) \tag{60}$$

$$J_{\mathrm{RP}} = \max_\omega \mu_{\hat{\Delta}}(N(j\omega)) \tag{61}$$

The three cost functions were evaluated on the augmented system closed in loop with controllers A, B, C; results are reported in Table 14 for all design points. In particular, for each controller and each design point, the cost function value reported in column J_{RP} [see Eq. (61)] coincides with the optimal cost function value of Eq. (55) achieved in the synthesis stage; that is, the robust performance requirement imposed by design is driving the optimization. On the other hand, the other two cost functions are simply evaluated a posteriori; in virtue of the properties of μ, $J_{\mathrm{RS}} \leq J_{\mathrm{RP}}$ and $J_{\mathrm{NP}} \leq J_{\mathrm{RP}}$ (i.e., RP implies RS and NP; see [10]).

Some remarks about cost function values follow:

Table 11 SCAS parameter values: controller *A*

Gain	90	70	50	30	15	0	CLEAN
k_{flelv}	n.d.	85.94	85.94	46.83	36.28	31.75	55.50
k_{pwelv}	n.d.	41.75	41.03	60.21	68.75	0.00	0.00
$k_{p\theta}$	n.d.	−50.00	−100.00	−150.00	−150.00	−86.06	−70.00
$k_{i\theta}$	n.d.	−29.08	−70.00	−100.00	−100.00	−69.18	−14.53

n.d. = not defined.

Table 12 SCAS parameter values: controller *B*

Gain	90	70	50	30	15	0	CLEAN
k_{flelv}	n.d.	85.94	27.99	46.73	41.45	48.59	43.11
k_{pwelv}	n.d.	42.60	45.78	57.10	68.75	0.00	0.00
$k_{p\theta}$	n.d.	−50.00	−100.00	−150.00	−150.00	−100.00	−70.00
$k_{i\theta}$	n.d.	−28.92	−70.00	−100.00	−100.00	−64.35	−15.99

Table 13 SCAS parameter values: controller *C*

Gain	90	70	50	30	15	0	CLEAN
k_{flelv}	n.d.	171.89	171.89	171.89	171.89	49.78	70.73
k_{pwelv}	n.d.	53.76	137.51	104.30	39.70	0.00	0.00
$k_{p\theta}$	n.d.	−62.56	−191.86	−259.09	−300.00	−101.40	−93.62
$k_{i\theta}$	n.d.	−37.26	−108.32	−144.88	−135.91	−65.37	−19.31

Table 14 Cost function values: controllers *A*, *B*, and *C*

	A			*B*			*C*		
	J_{RS}	J_{NP}	J_{RP}	J_{RS}	J_{NP}	J_{RP}	J_{RS}	J_{NP}	J_{RP}
CLEAN	0.703	0.864	0.954	0.688	0.863	0.970	0.731	0.850	0.956
0	1.021	0.410	1.046	1.069	0.812	1.174	1.073	0.810	1.166
15	0.359	0.744	0.881	0.361	1.389	1.478	0.340	0.919	0.960
30	0.597	0.654	0.944	0.597	1.198	1.464	0.669	0.853	0.989
50	0.764	0.299	0.926	0.785	1.322	1.796	0.706	0.895	1.167
70	0.752	0.434	0.989	0.754	0.602	1.109	0.816	0.592	0.999

1) For controller A, J_{RP} is always below 1 (except for the condition at $\tau_w = 0$), suggesting that original performance requirements (WP0) can be robustly achieved, even in presence of the current gain bound constraints (BND0).

2) Controller B is not able to achieve robust performance in most conditions (i.e., $J_{\mathrm{RP}} > 1$), with relatively large violation: this highlights a limitation on the achievable performance, imposed by the current bounds (BND0) on gain values.

3) Controller C is able to achieve robust performance in most conditions, except for conditions $\tau_w = 0$ and $\tau_w = 50$, with small violation. This means that, if the gain bounds can be relaxed by obtaining precise models for actuators and aircraft dynamics, the control performance can be improved by using large gains.

4) All controllers, at condition $\tau_w = 0$, yield $J_{\mathrm{RS}} > 1$; i.e., robust stability is not met; this is believed to be due to a very large amount of uncertainty in this particular condition. This implies $J_{\mathrm{RP}} > 1$; still, the violation is relatively small (below 1.1) and occurs at high frequency.

B. Comparison with Other Synthesis Methods

The method used to solve the structured μ-synthesis problem considered in this paper, described in Sec. V.C and based on the work of [26], was compared with other synthesis approaches, in order to show the effectiveness of the proposed method.

In particular, the structured μ-synthesis approaches taken into account for comparison are as follows:

1) First is the method proposed in this paper, which is based on the work of [26], which consists in reformulating the structured μ-synthesis problem as a structured H_∞ problem where the controller gains and the scalings are simultaneously optimized (hence referred to as the "simultaneous optimization approach").

2) Next is the $D-K$ approach to μ-synthesis [10], which in the case of structured μ-synthesis is formulated as an iteration of μ analysis (D step) and structured H_∞ controller synthesis (K step).

3) Third is the approach proposed by [32], which exploits relaxation techniques on the set of uncertainty to solve the structured μ-synthesis problem in presence of real and full block complex uncertainties as a structured H_∞ problem.

In the following, only the first two approaches are considered for comparison for simplicity.

The method of [26] was implemented in MATLAB by resorting to the systune routine, which in turn is based on the nonsmooth optimization methods described in [27]. $D-K$ iteration was implemented by using the musyn routine, which was introduced in MATLAB R2019b: this routine implements an iteration of μ-analysis and structured H_∞ synthesis; the latter is carried out by means of the MATLAB hinfstruct routine, again based on [27]. The computation of upper and lower bounds on μ in the robustness analysis [see Eqs. (59–61)] was carried out by means of the MATLAB mussv routine.

The two synthesis approaches were applied for each of the design points listed in Table 3, and for each of the performance requirements defined in Table 9. As a result, for each of the controllers A, B, C and for each design point, two values are obtained for the controller gains: one for the simultaneous optimization approach and one for the $D-K$ approach.

To carry out a fair comparison between the two methods, the optimization options reported in Table 15 were imposed in both the cases. In particular, as for the scaling order, in the simultaneous optimization approach this was fixed to a value of 3, whereas the musyn progressively increases the scaling order up to the maximum value if needed.

The optimization was run on a laptop featuring an Intel Core i5 CPU (dual core, 1.80 GHz) and 4 GB RAM. The code was run on MATLAB R2019b release. A summary of the execution time needed to solve the synthesis problem for one design point is reported in Table 16. The mean execution time for the $D-K$ iteration approach (i.e., the musyn routine) is one order of magnitude above the time employed by the simultaneous optimization approach (i.e., the systune routine).

In the following, only results related to controller A will be shown for conciseness, although similar results are obtained for the other

Table 15 Optimization options used for synthesis

Number of random starts	5(+1 by default)
Frequency range	1×10^{-2} to 1×10^{2} rad/s
Maximum scaling order	3

Table 16 Computational cost for one design point

Execution time, s	Simultaneous optimization	$D-K$ iteration
Mean	4.23	72.3
Minimum	3.15	53.8
Maximum	5.99	127.6

controllers. The values of the gains obtained with the two synthesis approaches for controller *A* are reported in Table 17, for each design point; in each cell, the first row reports the tuned value obtained with the simultaneous optimization approach (i.e., the value reported in Table 11, here reported for convenience), whereas the second row reports the value obtained by means of $D-K$ iteration, and the third row reports the relative difference with respect to the former approach.

An evaluation of robustness metrics defined in Eqs (59–61) was carried out a posteriori on the closed-loop system; the values of the evaluated metrics are reported in Table 18 for controller *A*. For each cell, the value of the metric obtained with the controller gains from simultaneous optimization is reported on the first row (which is the value reported in the corresponding part of Table 14), whereas the metric obtained with $D-K$ iteration is reported on the second row, along with the relative difference with respect to the former value. The robustness metrics were evaluated on a frequency grid of 300 points in the same range indicated in Table 15.

It can be noticed from Table 18 that in some design points the cost function achieved by means of the two approaches is comparable, whereas in other design points the $D-K$ iteration approach achieves cost function values much higher than the simultaneous optimization approach. A comparison with Table 17 reveals that the same design points where the gain values are significantly different also correspond to the points where the cost function values increase: this happens for design points $\tau_w = 70, 0$, and CLEAN.

Intuitively, one expects that the $D-K$ iteration approach is suboptimal with respect to the simultaneous optimization approach, because the set of parameters to be tuned is split in two subsets, which are alternatively optimized while keeping the other subset fixed. This is what actually happens for some of the design points, in particular $\tau_w = 50, 30$, and 15: for these design points, the cost function J_{RP} (which is the one minimized during the synthesis stage) is very similar, with the value obtained by means of $D-K$ iteration being slightly larger than the value achieved by simultaneous optimization, and with gain values practically identical.

Table 18 Robustness metrics, a posteriori analysis: controller *A*

	J_{RS}	J_{NP}	J_{RP}
CLEAN	0.703	0.864	0.954
	0.705 (+0.3%)	1.188 (+37.5%)	1.371 (+43.8%)
0	1.021	0.410	1.046
	4.349 (+325.8%)	1.314 (+220.5%)	5.590 (+434.3%)
15	0.359	0.744	0.881
	0.359 (−0.0%)	0.747 (+0.4%)	0.885 (+0.5%)
30	0.597	0.654	0.944
	0.597 (+0.0%)	0.657 (+0.4%)	0.944 (+0.0%)
50	0.764	0.299	0.926
	0.768 (+0.5%)	0.301 (+0.8%)	0.933 (+0.8%)
70	0.752	0.434	0.989
	0.840 (+11.8%)	0.471 (+8.4%)	1.098 (+11.0%)

Comparison between simultaneous optimization on first line and $D-K$ iteration on second line (relative difference in parentheses).

For other design points, $D-K$ iteration achieves totally different solutions with respect to the simultaneous optimization approach, and much larger values in terms of robust performance metric. This means that in these conditions $D-K$ iteration fails in achieving the same solution obtained by means of simultaneous optimization.

C. Verification on Linear Model

A comparison is carried out among the closed-loop systems associated with different controllers; for each design point, the SCAS obtained for that point is closed in loop with the linearized nominal model (N) and with the perturbed models (P1, P2), according to Table 3. The comparison is carried out in the frequency domain and in the time domain, showing, respectively, the sensitivity function $S_\theta(s)$ and the response of the pitch angle θ to a pilot step input $\delta_{\theta\mathrm{stick}}$.

Figures 10 and 11 show a comparison between the closed-loop systems associated with the baseline and *A* controllers, taking the condition $\tau_w = 15$ as an example; the solid-line plots represent the responses obtained in the nominal condition, and the dashed and dotted lines correspond to perturbed conditions. The plot of the inverse of the weighting function $W_{S,k}(s)$ for performance requirement WP0 at the same design point is shown in order to verify that, even in perturbed conditions, controller *A* satisfies robust performance in the parametric sense. It can be noticed that the shape of sensitivity function magnitude is similar for the two controllers, indicating a similar level of performance. The shape of the time response is similar, as well, although the shape of the baseline controller response is slightly worse than controller *A*.

Table 17 SCAS parameter values: controller *A*

Gain	90	70	50	30	15	0	CLEAN
k_{flelv}	n.d.	85.94	85.94	46.83	36.28	31.75	55.50
	n.d.	85.94	85.94	48.49	36.07	0.00	57.30
	n.d.	(+0.0%)	(+0.0%)	(+3.5%)	(−0.6%)	(−100.0%)	(+3.2%)
k_{pwelv}	n.d.	41.75	41.03	60.21	68.75	0.00	0.00
	n.d.	68.75	40.69	57.67	68.75	0.00	0.00
	n.d.	(+64.7%)	(−0.8%)	(−4.2%)	(+0.0%)	(−)	(−)
$k_{p\theta}$	n.d.	−50.00	−100.00	−150.00	−150.00	−86.06	−70.00
	n.d.	−50.00	−100.00	−150.00	−150.00	−100.00	−70.00
	n.d.	(+0.0%)	(+0.0%)	(+0.0%)	(+0.0%)	(−16.2%)	(+0.0%)
$k_{i\theta}$	n.d.	−29.08	−70.00	−100.00	−100.00	−69.18	−14.53
	n.d.	−40.00	−70.00	−100.00	−100.00	−100.00	−70.00
	n.d.	(−37.5%)	(−0.0%)	(+0.0%)	(+0.0%)	(−44.6%)	(−381.8%)

Comparison between simultaneous optimization (first row), $D-K$ iteration (second row), and relative difference (third row, in parentheses).

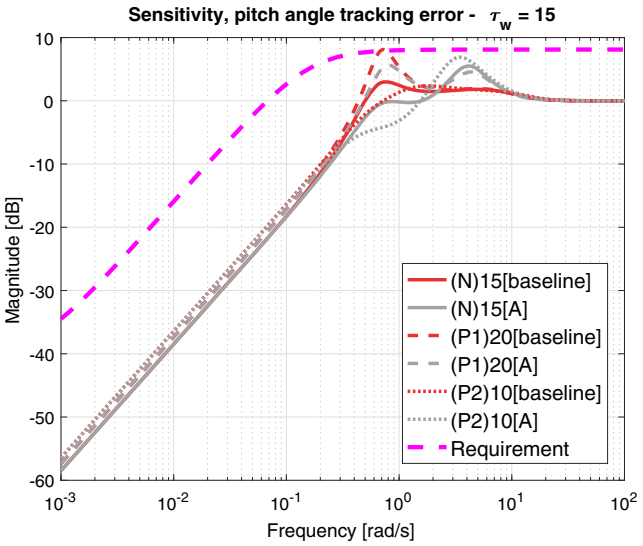

Fig. 10 Frequency domain comparison between baseline and *A* controllers. Pitch sensitivity function at $\tau_w = 15$.

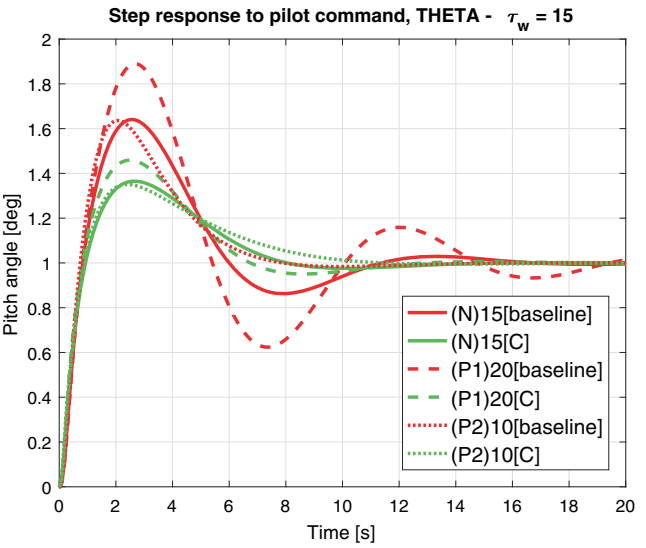

Fig. 12 Time domain comparison between baseline and *C* controllers. Pitch angle response to a pilot step input, $\tau_w = 15$.

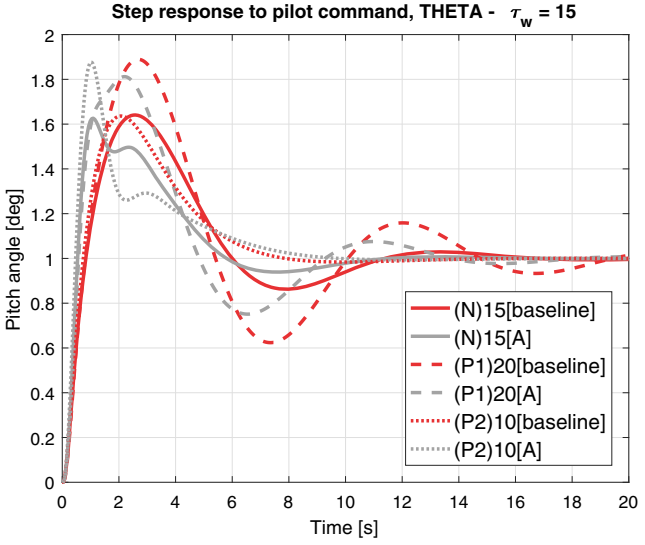

Fig. 11 Time domain comparison between baseline and *A* controllers. Pitch angle response to a pilot step input, $\tau_w = 15$.

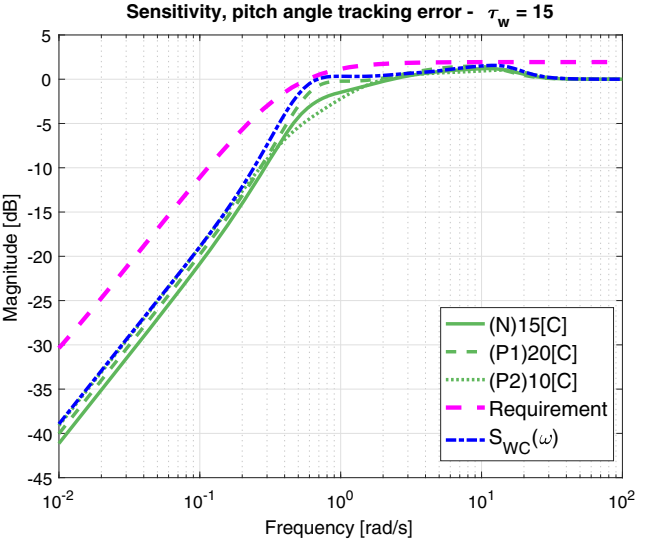

Fig. 13 Sensitivity function with worst-case upper bound. Controller *C*, design point $\tau_w = 15$.

The controller *C* was conceived with the rationale to explore the possibility to improve closed-loop performance by relaxing controller gain bounds; indeed, relaxed constraints on controller gain values would allow for a less stringent performance tradeoff. It is remarked that, at the current moment, the possibility to implement controller gains exceeding the original bounds BND0 on the actual SCAS is excluded; though, this study is meant to demonstrate the potential of the μ-synthesis approach.

Figure 12 shows a comparison of pitch angle reference step responses in nominal and perturbed conditions between baseline and *C* controllers, in the condition $\tau_w = 15$ as an example; performance improvement is evident in terms of reduced overshoot and better damping, as a result of relaxing bounds on SCAS gain values.

Figure 13 shows the sensitivity function evaluated on the *C* controller at nominal and perturbed conditions at design point $\tau_w = 15$; in addition, the inverse of the performance weight corresponding to performance level WP1 is plotted, along with the worst-case upper bound on sensitivity [see Eq. (38)]. The upper bound being below the performance requirement indicates that robust performance is achieved, consistently with the results of Table 14. Moreover, it is verified that the sensitivity magnitude, both in nominal and in perturbed conditions, is always below the worst-case upper bound; in this sense, the nonparametric analysis is consistent with the parametric one, and the parametric uncertainty description represents a subset of all possible perturbed models described by the nonparametric uncertainty description. The parametric robust performance analysis shows that the sensitivity magnitude in the perturbed cases is close to the nonparametric worst-case upper bound, for most of the design points: this suggests that the nonparametric uncertainty description is tight (i.e., nonconservative). Figure 14 shows the same plot in the condition $\tau_w = 70$, which is subject to a larger amount of uncertainty: the worst-case upper bound is less tight; though, robust performance is still achieved.

D. Nonlinear Simulation Results

Finally, human-in-the-loop piloted simulations were conducted on a nonlinear QTW model closed in loop with the *A* controller, with the objective of verifying the applicability of the controller for all wing tilt angles (including transition) in a high-fidelity simulation environment. The validation of the design by means of nonlinear simulations is necessary because, as stated in the Introduction, the considered controller design methodology does not provide any guarantee about stability and performance of the closed-loop system when transitioning between design points. The QTW model features

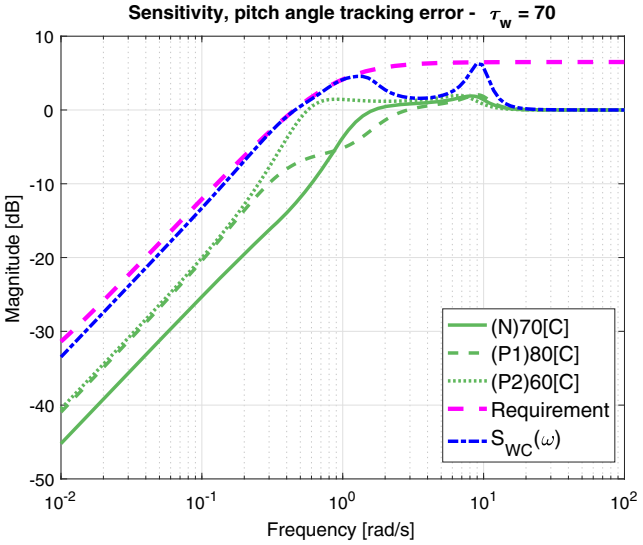

Fig. 14 Sensitivity function with worst-case upper bound. Controller C, design point $\tau_w = 70$.

nonlinear equations of motion and a Dryden wind gust disturbance model; no actuator saturation or rate saturation is present. The gain values of the controller A were implemented in the longitudinal SCAS, whereas the baseline gain values were maintained in the lateral-directional SCAS.

The mission profile consisted in a full conversion from hover ($\tau_w = 90$) to airplane mode ($\tau_w = \text{CLEAN}$), and back again to helicopter mode. Results are shown in Fig. 15; in the first part of the simulation, no wind disturbance is present; the disturbance is injected at time 208 s, with an root mean square (RMS) of the driving noise input of 0.5 m/s. It was possible for the pilot to fly the QTW with acceptable workload; no instability issues were found out in the simulation. Performance was qualitatively comparable to the one obtained by means of the baseline controller. It is pointed out that significant oscillations occurred in the roll axis in presence of wind, in the condition $\tau_w = 50$ (see Fig. 15, from 400s on); this issue was accepted in flight tests; however, it was already known and is due to degraded performance of the lateral-directional baseline SCAS at those operating conditions.

VII. Conclusions

A structured μ-synthesis-based approach to attitude controller design was proposed and applied to the tuning of QTW-UAV longitudinal SCAS gains, guaranteeing robust performance with respect to uncertainty in the operating conditions. By means of the proposed approach, it was possible to obtain a solution with performance comparable to the one achieved by the baseline controller, remaining in the same controller parameters search space. At the same time, the proposed approach guarantees robust performance with respect to the considered nonparametric uncertainty description, whereas the baseline solution only guarantees robust performance with respect to parametric uncertainty. The proposed approach does not guarantee any stability and performance robustness property during the transition between design points; for this reason, it is necessary to carry out simulations on a nonlinear model to validate the design.

The synthesis approach proposed in the paper (simultaneous optimization of gains and scalings) was compared with a different approach to structured μ-synthesis (namely, $D-K$ iteration). The proposed approach turned out to be superior in terms of computational effort and optimality of the solution; in some design point, $D-K$ iteration failed in finding a solution comparable to the simultaneous optimization approach.

Furthermore, a limitation in the achievable performance, due to the current stringent gain bounds, is demonstrated. The possibility of improving performance with respect to the baseline solution is explored; more aggressive requirements on robust performance can be achieved, provided that the bounds on controller gains are relaxed.

The novel worst-case sensitivity upper bound tool turned out to provide an intuitive graphical interpretation of performance robustness and of worst-case performance in the frequency domain, which can be complemented to the Bode magnitude diagram of the nominal closed-loop transfer function.

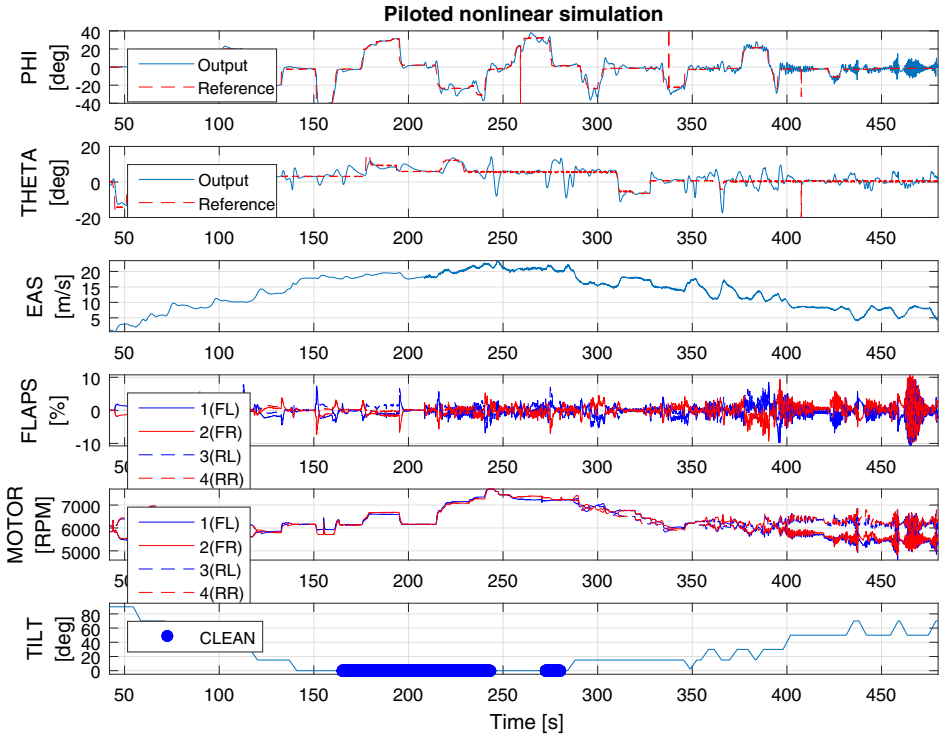

Fig. 15 Nonlinear simulation results.

Appendix: State-Space Models Matrices

In this Appendix, the matrices of the models of the open-loop system in state-space form are reported from [6] for all the operating points reported in Table 2. With reference to Fig. 2, the system in state-space form contains the blocks $G_{\text{lon}}(s;\tau_w)$ (i.e., the bare airframe dynamics), the two blocks $1/T_a s+1$ and $1/T_{\text{th}} s+1$ (i.e., the actuators dynamics), and the block $K_{\text{lon}}(\tau_w)$ (i.e., the PFCS). The input vector is $u=[\delta_{\text{flelv}_{CP}},\delta_{\text{pwelv}_{CP}},\delta_{\text{th}_{CP}}]^T$, and the state vector is $x=[u,w,q,\theta,\delta_{\text{flelv}},\delta_{\text{pwelv}},\delta_{\text{th}}]^T$. The matrices are reported in the form $[A|B]$, with the state equation being $\dot{x}=Ax+\text{Bu}$.

$$\left[\begin{array}{ccccccc|ccc}
-0.632 & 0.018 & 0.033 & -9.801 & -0.0146 & 0.0096 & -0.0005 & 0 & 0 & 0\\
0.054 & 0.19 & 1 & 0.321 & 0 & -0.0065 & -0.2935 & 0 & 0 & 0\\
0.755 & -0.922 & 0.026 & 0 & 0.0024 & -0.8966 & 0.0044 & 0 & 0 & 0\\
0 & 0 & 1 & 0 & 0 & 0 & 0 & 0 & 0 & 0\\
0 & 0 & 0 & 0 & -20 & 0 & 0 & 0 & 0 & 0\\
0 & 0 & 0 & 0 & 0 & -6.67 & 0 & 0 & 2 & 0\\
0 & 0 & 0 & 0 & 0 & 0 & -6.67 & 0 & 0 & 6.67
\end{array}\right] \quad (\tau_w = 90)$$

$$\left[\begin{array}{ccccccc|ccc}
-1.375 & -0.643 & 0.015 & -9.807 & -0.0122 & 0.05 & 0.0492 & 0 & 0 & 0\\
0.16 & -0.389 & 2.445 & -0.024 & 0.0022 & -0.0185 & -0.2926 & 0 & 0 & 0\\
1.685 & -0.633 & 0.276 & 0 & -0.0166 & -0.9396 & -0.024 & 0 & 0 & 0\\
0 & 0 & 1 & 0 & 0 & 0 & 0 & 0 & 0 & 0\\
0 & 0 & 0 & 0 & -20 & 0 & 0 & 0.76 & 0 & 0\\
0 & 0 & 0 & 0 & 0 & -6.67 & 0 & 0 & 2 & 0\\
0 & 0 & 0 & 0 & 0 & 0 & -6.67 & 0 & 0 & 6.67
\end{array}\right] \quad (\tau_w = 80)$$

$$\left[\begin{array}{ccccccc|ccc}
-0.638 & 0.357 & 0.113 & -9.802 & -0.0069 & 0.113 & 0.0354 & 0 & 0 & 0\\
-0.908 & -1.271 & 4.919 & 0.296 & 0.0069 & -0.0287 & -0.2284 & 0 & 0 & 0\\
0.413 & -0.039 & -0.085 & 0 & -0.0066 & -0.9614 & 0.0073 & 0 & 0 & 0\\
0 & 0 & 1 & 0 & 0 & 0 & 0 & 0 & 0 & 0\\
0 & 0 & 0 & 0 & -20 & 0 & 0 & 1.52 & 0 & 0\\
0 & 0 & 0 & 0 & 0 & -6.67 & 0 & 0 & 1.72 & 0\\
0 & 0 & 0 & 0 & 0 & 0 & -6.67 & 0 & 0 & 6.67
\end{array}\right] \quad (\tau_w = 70)$$

$$\left[\begin{array}{ccccccc|ccc}
-0.387 & -0.077 & 0.261 & -9.799 & -0.0136 & 0.1465 & 0.0191 & 0 & 0 & 0\\
-0.075 & -0.919 & 6.991 & 0.392 & -0.0053 & 0.0602 & -0.3026 & 0 & 0 & 0\\
-0.276 & -0.033 & -0.004 & 0.005 & -0.0307 & -0.8223 & 0.0827 & 0 & 0 & 0\\
0 & 0 & 1 & 0 & 0 & 0 & 0 & 0 & 0 & 0\\
0 & 0 & 0 & 0 & -20 & 0 & 0 & 1.52 & 0 & 0\\
0 & 0 & 0 & 0 & 0 & -6.67 & 0 & 0 & 1.43 & 0\\
0 & 0 & 0 & 0 & 0 & 0 & -6.67 & 0 & 0 & 6.67
\end{array}\right] \quad (\tau_w = 60)$$

$$\left[\begin{array}{ccccccc|ccc}
-0.735 & -0.129 & -0.199 & -9.804 & -0.0161 & 0.1289 & 0.0818 & 0 & 0 & 0\\
-0.371 & -0.533 & 8.029 & -0.224 & -0.0141 & 0.0715 & -0.2585 & 0 & 0 & 0\\
-0.488 & 0.18 & 0.107 & -0.005 & -0.0809 & -0.6957 & 0.094 & 0 & 0 & 0\\
0 & 0 & 1 & 0 & 0 & 0 & 0 & 0 & 0 & 0\\
0 & 0 & 0 & 0 & -20 & 0 & 0 & 1.52 & 0 & 0\\
0 & 0 & 0 & 0 & 0 & -6.67 & 0 & 0 & 1.15 & 0\\
0 & 0 & 0 & 0 & 0 & 0 & -6.67 & 0 & 0 & 6.67
\end{array}\right] \quad (\tau_w = 50)$$

$$\left[\begin{array}{ccccccc|ccc} -0.884 & 0.063 & -0.099 & -9.806 & -0.0209 & 0.1388 & 0.1259 & 0 & 0 & 0 \\ -0.615 & -0.411 & 9.543 & -0.095 & -0.0361 & 0.1337 & -0.2158 & 0 & 0 & 0 \\ -0.95 & 0.12 & 0.169 & -0.002 & -0.1431 & -0.5668 & 0.1519 & 0 & 0 & 0 \\ 0 & 0 & 1 & 0 & 0 & 0 & 0 & 0 & 0 & 0 \\ 0 & 0 & 0 & 0 & -20 & 0 & 0 & 2.36 & 0 & 0 \\ 0 & 0 & 0 & 0 & 0 & -6.67 & 0 & 0 & 0.87 & 0 \\ 0 & 0 & 0 & 0 & 0 & 0 & -6.67 & 0 & 0 & 6.67 \end{array}\right] \quad (\tau_w = 40)$$

$$\left[\begin{array}{ccccccc|ccc} -0.669 & -0.115 & -0.076 & -9.806 & -0.0164 & 0.1079 & 0.1182 & 0 & 0 & 0 \\ -0.329 & -1.145 & 10.943 & -0.062 & -0.0245 & 0.1841 & -0.2563 & 0 & 0 & 0 \\ -0.724 & 0.081 & -0.432 & 0 & -0.3043 & -0.3845 & 0.1336 & 0 & 0 & 0 \\ 0 & 0 & 1 & 0 & 0 & 0 & 0 & 0 & 0 & 0 \\ 0 & 0 & 0 & 0 & -20 & 0 & 0 & 3.2 & 0 & 0 \\ 0 & 0 & 0 & 0 & 0 & -6.67 & 0 & 0 & 0.87 & 0 \\ 0 & 0 & 0 & 0 & 0 & 0 & -6.67 & 0 & 0 & 6.67 \end{array}\right] \quad (\tau_w = 30)$$

$$\left[\begin{array}{ccccccc|ccc} -0.839 & -0.035 & -0.169 & -9.806 & -0.0157 & 0.0443 & 0.1541 & 0 & 0 & 0 \\ -0.426 & -1.752 & 12.98 & -0.112 & -0.0082 & 0.2086 & -0.2038 & 0 & 0 & 0 \\ -1.065 & -0.103 & -0.41 & 0 & -0.4424 & -0.2031 & 0.1908 & 0 & 0 & 0 \\ 0 & 0 & 1 & 0 & 0 & 0 & 0 & 0 & 0 & 0 \\ 0 & 0 & 0 & 0 & -20 & 0 & 0 & 3.2 & 0 & 0 \\ 0 & 0 & 0 & 0 & 0 & -6.67 & 0 & 0 & 0.58 & 0 \\ 0 & 0 & 0 & 0 & 0 & 0 & -6.67 & 0 & 0 & 6.67 \end{array}\right] \quad (\tau_w = 20)$$

$$\left[\begin{array}{ccccccc|ccc} -0.612 & -0.046 & 0.026 & -9.807 & -0.0121 & 0.0543 & 0.1336 & 0 & 0 & 0 \\ -0.717 & -1.348 & 14.118 & 0.046 & -0.0788 & 0.2016 & -0.1495 & 0 & 0 & 0 \\ -0.674 & -0.015 & -0.25 & 0 & -0.5463 & -0.1084 & 0.1454 & 0 & 0 & 0 \\ 0 & 0 & 1 & 0 & 0 & 0 & 0 & 0 & 0 & 0 \\ 0 & 0 & 0 & 0 & -20 & 0 & 0 & 3.22 & 0 & 0 \\ 0 & 0 & 0 & 0 & 0 & -6.67 & 0 & 0 & 0.29 & 0 \\ 0 & 0 & 0 & 0 & 0 & 0 & -6.67 & 0 & 0 & 6.67 \end{array}\right] \quad (\tau_w = 15)$$

$$\left[\begin{array}{ccccccc|ccc} -0.559 & -0.224 & -0.421 & -9.803 & -0.0073 & 0.027 & 0.1512 & 0 & 0 & 0 \\ -0.825 & -0.96 & 14.548 & -0.267 & -0.0979 & 0.1552 & -0.0998 & 0 & 0 & 0 \\ -0.422 & 0.374 & -0.434 & 0.001 & -0.6809 & -0.0715 & 0.0763 & 0 & 0 & 0 \\ 0 & 0 & 1 & 0 & 0 & 0 & 0 & 0 & 0 & 0 \\ 0 & 0 & 0 & 0 & -20 & 0 & 0 & 3.48 & 0 & 0 \\ 0 & 0 & 0 & 0 & 0 & -6.67 & 0 & 0 & 0 & 0 \\ 0 & 0 & 0 & 0 & 0 & 0 & -6.67 & 0 & 0 & 6.67 \end{array}\right] \quad (\tau_w = 10)$$

$$\left[\begin{array}{ccccccc|ccc} -0.7 & 0.485 & -0.88 & -9.795 & 0.0012 & 0.0116 & 0.1844 & 0 & 0 & 0 \\ -0.567 & -3.818 & 18.113 & -0.474 & -0.1502 & 0.1574 & -0.0641 & 0 & 0 & 0 \\ -0.068 & 0.255 & -4.318 & 0.036 & -1.1085 & 0.0516 & 0.0334 & 0 & 0 & 0 \\ 0 & 0 & 1 & 0 & 0 & 0 & 0 & 0 & 0 & 0 \\ 0 & 0 & 0 & 0 & -20 & 0 & 0 & 4 & 0 & 0 \\ 0 & 0 & 0 & 0 & 0 & -6.67 & 0 & 0 & 0 & 0 \\ 0 & 0 & 0 & 0 & 0 & 0 & -6.67 & 0 & 0 & 6.67 \end{array}\right] \quad (\tau_w = 0)$$

$$\left[\begin{array}{ccccccc|ccc} -0.762 & 0.562 & -1.537 & -9.785 & 0.0615 & -0.0012 & 0.2096 & 0 & 0 & 0 \\ -0.176 & -4.28 & 22.922 & -0.646 & -0.1554 & 0.0971 & -0.0867 & 0 & 0 & 0 \\ 0.097 & -0.883 & -4.805 & 0.044 & -1.6483 & 0.0277 & 0.0059 & 0 & 0 & 0 \\ 0 & 0 & 1 & 0 & 0 & 0 & 0 & 0 & 0 & 0 \\ 0 & 0 & 0 & 0 & -20 & 0 & 0 & 4 & 0 & 0 \\ 0 & 0 & 0 & 0 & 0 & -6.67 & 0 & 0 & 0 & 0 \\ 0 & 0 & 0 & 0 & 0 & 0 & -6.67 & 0 & 0 & 6.67 \end{array}\right] \quad (\tau_w = \text{CLEAN})$$

References

[1] Muraoka, K., Okada, N., and Kubo, D., "Quad Tilt Wing VTOL UAV: Aerodynamic Characteristics and Prototype Flight Test," *AIAA Infotech@Aerospace Conference*, AIAA Paper 2009-1834, 2009. https://doi.org/10.2514/6.2009-1834

[2] Sato, M., and Muraoka, K., "Flight Controller Design and Demonstration of Quad-Tilt-Wing Unmanned Aerial Vehicle," *Journal of Guidance, Control, and Dynamics*, Vol. 38, No. 6, 2015, pp. 1071–1082. https://doi.org/10.2514/1.G000263

[3] Cetinsoy, E., Dikyar, S., Hancer, C., Oner, K., Sirimoglu, E., Unel, M., and Aksit, M., "Design and Construction of a Novel Quad Tilt-Wing UAV," *Mechatronics*, Vol. 22, No. 6, 2012, pp. 723–745. https://doi.org/10.1016/j.mechatronics.2012.03.003

[4] Abhishek, A., Krishna, M., Sinha, S., Bhowmik, J., and Das, D., "Design, Development and Flight Testing of a Novel Quadrotor Convertiplane Unmanned Air Vehicle," *73rd Annual Forum of the American Helicopter Society*, AHS International, Inc., Fairfax, VA, 2017, Paper 156.

[5] Totoki, H., Ochi, Y., Sato, M., and Muraoka, K., "Design and Testing of a Low-Order Flight Control System for Quad-Tilt-Wing UAV," *Journal of Guidance, Control, and Dynamics*, Vol. 39, No. 10, 2016, pp. 2423–2430. https://doi.org/10.2514/1.G001577

[6] Sato, M., and Muraoka, K., "Flight Controller Design for Small Quad-Tilt-Wing UAV," *Journal of the Japan Society for Aeronautical and Space Sciences*, Vol. 64, No. 1, 2016, pp. 79–82 (in Japanese). https://doi.org/10.2322/jjsass.64.79

[7] Ackermann, J., "Multi-Model Approaches to Robust Control System Design," *Uncertainty and Control*, Vol. 70, Lecture Notes in Control and Information Sciences, Springer, Berlin, 1985, pp. 108–130. https://doi.org/10.1007/BFb0007282

[8] Nami, C., Oka, K., Sato, M., Harada, A., and Muraoka, K., "H_∞ Control-Based Robust CAS Design for QTW-UAV via the Multiple-Model Approach with Particle Swarm Optimization," *International Journal of Aerospace Engineering*, Vol. 2019, July 2019, Paper 9267059. https://doi.org/10.1155/2019/9267059

[9] Maruta, I., Kim, T., and Sugie, T., "Fixed-Structure H_∞ Controller Synthesis: A Meta-Heuristic Approach Using Simple Constrained Particle Swarm Optimization," *Automatica*, Vol. 45, No. 2, 2009, pp. 553–559.

[10] Skogestad, S., and Postlethwaite, I., *Multivariable Feedback Control: Analysis and Design*, Wiley, New York, 1996, Chap. 8.

[11] Zhou, K., Doyle, J., and Glover, K., *Robust and Optimal Control*, Prentice Hall, Upper Saddle River, NJ, 1996, Chap. 9.

[12] Adams, R., and Banda, S., "Robust Flight Control Design Using Dynamic Inversion and Structured Singular Value Synthesis," *IEEE Transactions on Control Systems Technology*, Vol. 1, No. 2, 1993, pp. 80–92. https://doi.org/10.1109/87.238401

[13] Balas, G., and Packard, A., "Design of Robust, Time-Varying Controllers for Missile Autopilots," *IEEE Conference on Control Applications*, IEEE, New York, 1992, pp. 104–110. https://doi.org/10.1109/CCA.1992.269891

[14] Balas, G., Packard, A., Renfrow, J., Mullaney, C., and M'Closkey, R., "Control of the F-14 Aircraft Lateral-Directional Axis During Powered Approach," *Journal of Guidance, Control, and Dynamics*, Vol. 21, No. 6, 1998, pp. 899–908. https://doi.org/10.2514/2.4323

[15] Balas, G., Young, P., and Doyle, J., "The Process of Control Design for the NASA Langley Minimast Structure," *American Control Conference*, IEEE, New York, 1991, pp. 562–567. https://doi.org/10.23919/ACC.1991.4791434

[16] Buffington, J., Adams, R., and Banda, S., "Robust, Nonlinear, High Angle-of-Attack Control Design for a Supermaneuverable Vehicle," *Guidance, Navigation and Control Conference*, AIAA Paper 1993-3774, 1993. https://doi.org/10.2514/6.1993-3774

[17] Doyle, J., Lenz, K., and Packard, A., "Design Examples Using μ-Synthesis: Space Shuttle Lateral Axis FCS During Reentry," *Conference on Decision and Control*, IEEE, New York, 1986, pp. 2218–2223. https://doi.org/10.1109/CDC.1986.267482

[18] Ngo, A., Reigelsperger, W., Banda, S., and Bessolo, J., "Tailless Aircraft Control Law Design Using Dynamic Inversion μ-Synthesis," *IEEE International Conference on Control Applications*, IEEE, New York, 1996, pp. 107–112. https://doi.org/10.1109/CCA.1996.558615

[19] Reiner, J., Balas, G., and Garrard, W., "Flight Control Design Using Robust Dynamic Inversion and Time-Scale Separation," *Automatica*, Vol. 32, No. 11, 1996, pp. 1493–1504. https://doi.org/10.1016/S0005-1098(96)00101-X

[20] Sparks, A., and Banda, S., "Application of Structured Singular Value Synthesis to a Fighter Aircraft," *Journal of Guidance, Control, and Dynamics*, Vol. 16, No. 5, 1993, pp. 940–947. https://doi.org/10.2514/3.21105

[21] Mollov, L., Kralev, J., Slavov, T., and Petkov, P., "μ-Synthesis and Hardware-in-the-Loop Simulation of Miniature Helicopter Control System," *Journal of Intelligent and Robotic Systems*, Vol. 76, Feb. 2014, pp. 315–351. https://doi.org/10.1007/s10846-014-0033-x

[22] Menezes, E., Aguiar, R., Simoes, A., and Apkarian, P., "Structured Robust Controller Design via Non-Smooth Mixed μ-Synthesis," *IET Control Theory and Applications*, Vol. 10, No. 17, 2016, pp. 2186–2193. https://doi.org/10.1049/iet-cta.2016.0570

[23] Lesprier, J., Biannic, J.-M., and Roos, C., "Nonlinear Structured H_∞ Controllers for Parameter-Dependent Uncertain Systems with Application to Aircraft Landing," *IEEE Conference on Control Applications*, IEEE, New York, 2014, pp. 433–438. https://doi.org/10.1109/CCA.2014.6981384

[24] Lhachemi, H., Saussié, D., and Zhu, G., "A Structured H_∞-Based Optimization Approach for Integrated Plant and Self-Scheduled Flight Control System Design," *Aerospace Science and Technology*, Vol. 45, Sept. 2015, pp. 30–38. https://doi.org/10.1016/j.ast.2015.04.003

[25] Panza, S., Sato, M., Lovera, M., and Muraoka, K., "Robust Attitude Control Design of Quad-Tilt-Wing UAV: A Structured μ-Synthesis Approach," *IEEE Conference on Control Technology and Applications*, IEEE, New York, 2018, pp. 781–786. https://doi.org/10.1109/CCTA.2018.8511407

[26] Apkarian, P., "Nonsmooth μ Synthesis," *International Journal of Robust and Nonlinear Control*, Vol. 21, No. 13, 2011, pp. 1493–1508. https://doi.org/10.1002/rnc.1644

[27] Apkarian, P., and Noll, D., "Nonsmooth H_∞ Synthesis," *IEEE Transactions on Automatic Control*, Vol. 51, No. 1, 2006, pp. 71–86. https://doi.org/10.1109/TAC.2005.860290

[28] Marcos, A., and Sato, M., "Flight Testing of an Structured H-Infinity Controller: An EU-Japan Collaborative Experience," *IEEE Conference on Control Technology and Applications*, IEEE, New York, 2017, pp. 2132–2137. https://doi.org/10.1109/CCTA.2017.8062768

[29] Sato, M., and Satoh, A., "Flight Control Experiment of Multipurpose-Aviation-Laboratory-Alpha In-Flight Simulator," *Journal of Guidance, Control, and Dynamics*, Vol. 34, No. 4, 2011, pp. 1081–1096. https://doi.org/10.2514/1.52400

[30] Panza, S., "Structured Flight Control Law Design for Helicopters and Tiltrotors," Ph.D. Thesis, Politecnico di Milano, Dipartimento di Scienze e Tecnologie Aerospaziali, Milan, 2018.

[31] Berger, T., Ivler, C., Berrios, M., Tischler, M., and Miller, D., "Disturbance Rejection Handling Qualities Criteria for Rotorcraft," *72nd Annual Forum of the American Helicopter Society*, AHS International, Inc., Fairfax, VA, 2016, Paper 78.

[32] da Silva de Aguiar, R. S., Apkarian, P., and Noll, D., "Structured Robust Control Against Mixed Uncertainty," *IEEE Transactions on Control Systems Technology*, Vol. 26, No. 5, 2018, pp. 1771–1781. https://doi.org/10.1109/TCST.2017.2723864